Master´s Final Thesis

Industrial Engineering (Mechanical specialty)

Design, implementation and testing of a wire scanner prototype

MEMORANDUM

Author: Iñigo Ortiz de Viñaspre
                 Oriol Torta
Director: Ana Barjau
                 Juan Herranz
Call: Septiembre 2019

ETSEIB

Escola Tècnica Superior d'Enginyeria Industrial de Barcelona

UPC

ETSEIB

Summary

A wire scanner is an electro-mechanical device that measures the transverse profile of the particle beam circulating through a particle accelerator. The major source of errors in the scanner performance has been pinpointed as the mechanical vibrations of the system.

The main objective of this project is to study and understand the technology of a wire scanner and to develop a small-scale prototype of this device to make some experiments and measures with it.

The operation of a wire scanner is described, taking from reference the wire scanner of the LHC (Large Hadron Collider) located in CERN. The mechanical actuator used to drive the prototype mechanism is a piezoelectric linear actuator and viability study is carried out to find the possible mechanical solutions.

The dynamics of the system are characterized, modelling the wire scanner, defining the wire dynamic equations and designing a rotational motion pattern for the wire fork. A simulation is carried out using Matlab in order to predict the system response.

A mechanism for the wire scanner prototype is designed, constructed and assembled, with the different parts being modelled in 3D CAD and mechanized. An electronic experimental set-up is installed in order to drive the prototype and read the response of the system to the designed motion pattern.

Finally, some experimental tests are carried out to verify the system performance, identify possible sources of error and find solutions to help improving the prototype.

ETSEIB

Contents

ETSEIB

Figure list

ETSEIB

ETSEIB

Table List

1. Preface

1.1. Origin of the project

The LHC (Large Hadron Collider) located in CERN contains a wire scanner, an electro-mechanical device that measures the transverse profile of the particle beam circulating through the synchrotron. In the near future this measurement will require a much higher accuracy as the luminosity of the collider will be substantially increased, being the current precision of the scanner insufficient for the demanded task.

The major source of errors in the scanner performance has been pinpointed as the mechanical vibrations of the system, which induce important uncertainty in the wire position. Many papers have been written on this subject, as understanding, measuring and minimizing the wire vibrations will be key in the incoming improvement of the wire scanner.

This Final Master Project follows the line of investigation carried out in cooperation between the CERN Beams and Instrumentation department and the UPC Mechanical Engineering department, mostly conducted by Juan Herranz and Ana Barjau who also perform as the co-directors of this project. In his PhD Thesis [1], Juan Herranz identified the sources of error, developed a vibration measurement system and presented a new improved wire scanner prototype. The main results were published in two scientific papers, one devoted to the vibration measurements and calibrations [2], and the other focused on the dynamical models of the wire scanner [3].

The next logical step is the implementation of an optimized motion pattern, which may help avoiding undesired vibrations. In this regard, some work was already carried out in an undergraduate thesis [4], but much still remains to be done. This is the starting point where this project steps in, drawing upon all of the previous research and trying to take it into the next stated goal.

1.2. Motivation

The main motivation for this project is the chance of enlarging the general knowledge about the wire scanner behaviour and obtaining relevant results which might lead to the development of the next version of the system. As already mentioned, the accuracy of the scanner measurements needs a substantial improvement to fulfil the upcoming requirements, therefore any little enhancement that this project can provide will be of enormous value.

ETSEIB

On a personal level, the realisation of the project gave us a unique opportunity not to be missed. It gives us the chance of fulfilling aspirations that any engineer or scientist certainly has, as well as some of our own. Not many academic projects would allow us to contribute to real investigations, teaming up with experienced investigators and learning from them and their previous work.

Furthermore, cooperating with CERN is an incredible experience as it is one of the most prestigious scientific institutions worldwide, with lots of top tier investigations being performed in their facilities. Knowing that there is the possibility that our work contributes, even if humbly, in some way in the great physics discoveries to come, clearly motivates us to give the best of ourselves and to try to carry out the best possible project.

ETSEIB

2. Introduction

As said in the preface, this project is the direct continuation of the previous investigation done with the main aim of optimizing and minimizing the vibrations of the LHC wire scanner, therefore improving its accuracy. This work tries to carry out some improvement over the present knowledge through the achievement of some goals.

2.1. Objectives

The main goal of the project is to set up a system that allows vibration measurements to be made under different movement patterns.

To achieve this primary target, the following objectives have to be accomplished:

- To fully understand the previous work on the subject and the proper operation of the current wire scanner, and what is already known about its development.

- To design, calculate and implement a small-scale prototype that replicates the existing device, allowing measurements and experimentation without having to disassemble the LHC scanner.

- To implement and calibrate an adaptation of the vibration measurement system presented in **[2]** for the prototype setup.

- Finally, to scale the results to the real wire scanner for future use of the reached conclusions for improving and developing a new version of the system.

2.2. Scope

- **Project elements**
    - A scanner mechanism prototype
    - Planes of construction and assembly guide
    - A measure and signal conditioning electronic system
- **Milestones**
    1. Previous existing work study, March
    2. Prototype design, manufacture and assembly, June
    3. Get to know piezoelectric actuator and start up, May
    4. Measures taking, July
    5. Conclusions, September
- **Limits and exclusions**

ETSEIB

- Reuse all the possible elements available from previous works
- Actuator stroke limitations
- Objectives are limited to understand the dynamic behaviour of the prototype. We are not optimizing nor minimizing vibrations, as initially proposed. Along the project description is shown that those objectives are too ambitious.

3. Starting point

In order to develop the wire scanner prototype, there are two key aspects to be presented and described for proper understanding of the design process of system set up. The first one is the original LHC wire scanner, with its construction, functionality and desired performance. The other is the available hardware elements in the UPC Mechanical laboratory, given for the project both from previous work and by the CERN Beams and Instrumentation department.

3.1. The LHC wire scanner

The LHC wire scanner is an electro-mechanical device which measures the transverse beam profile in a particle accelerator by means of a thin wire moving in an intermittent manner. When the wire cuts the beam, it emits a stream of secondary particles and dispersed primary particles which are received by a sensor system (a scintillator coupled with a photomultiplier) that measures the light intensity. Additionally, a precision rotary potentiometer captures the wire position which, combined with the measured luminosity, allows the reconstruction of the transverse beam profile (Figure 3.1).
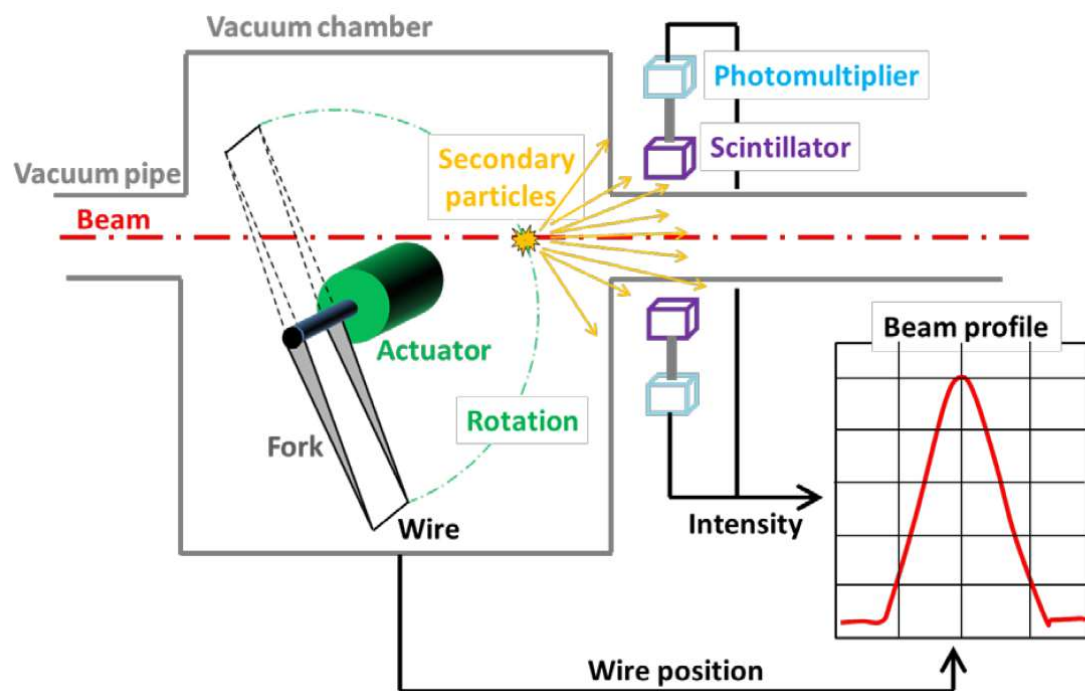
Figure 3.1:Schematics of the LHC wire scanner (from [1])

The fork motion is controlled by a motor. The motion pattern consists of three distinct phases: acceleration phase, constant speed phase (while the wire crosses the beam) and deceleration phase. This movement is realized twice per scan cycle with opposite sense (OUT-IN and IN-OUT), generating an intermittent motion (Figure 3.2).
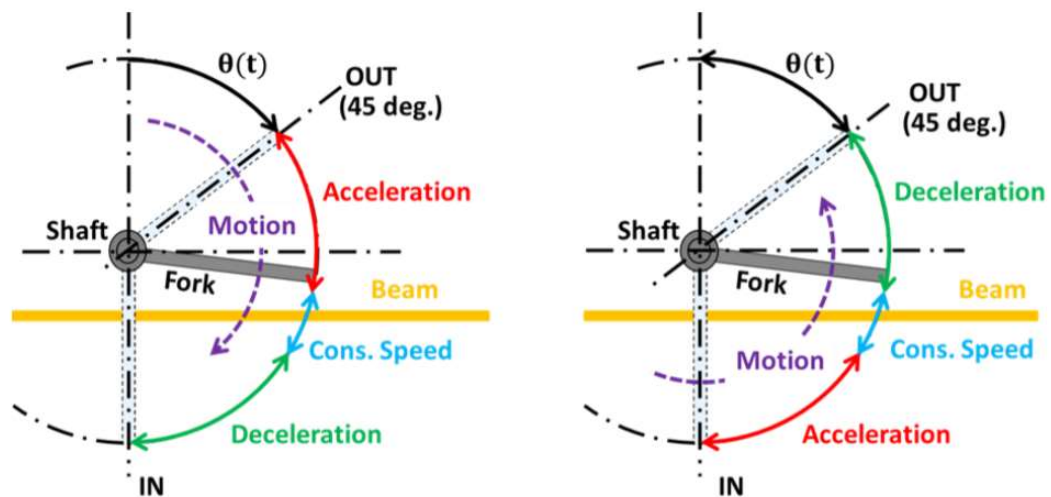
Figure 3.2: Qualitative description of the fork motion in a cycle (from [1])

The system has to meet two major requirements concerning the wire speed and measurement accuracy.

The requirement on the wire speed is associated with the fact that the wire gets damaged at the high temperatures achieved because of the beam energy deposition in the wire. Therefore, a high travelling speed reduces the duration of the energy deposition and consequently the wire heating. Previous studies [1] have determined that the desired wire speed should be no less than 20 m/s.

The measurement accuracy is key to reduce the uncertainty in the beam size determination, which should be less than 1,8% [1]. There are many sources of error in the whole system. In this project we will focus on the one associated with the actual wire motion. The high acceleration causes deflections and vibrations on the shaft, fork and wire, resulting in inconsistency between the real position of the wire and the one provided by the potentiometer (Figure 3.3).
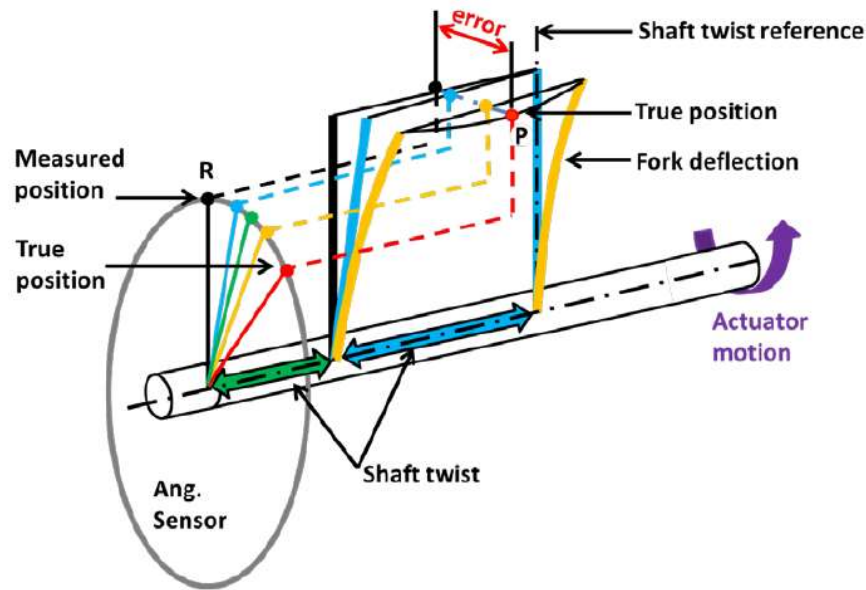
Figure 3.3: Schematics of the wire deflection in the measurement chain (from [1])

3.2. Initial available elements

Ideally, the measurements and experimentation would be done in the real LHC wire scanner. However, this is not a realistic possibility as the LHC is stopped in very few occasions and the authorization to disassemble any component is pretty demanded. For this reason, the objective is to build a system preserving some of the original scanner characteristics, though using the electromechanical elements available.

For the implementation of the small scale prototype there were some mechanical and electronic elements that could be appropriate in the Mechanical Laboratory of the UPC. Although it is not completely compulsory to use these elements and they are not enough by themselves, most of them are suitable for the project's purpose and form the basis to design and implement the replica system.

The Beams and Instrumentation department of the CERN provided the carbon wire, the actuator to drive the mechanism and the sensors and instruments required to carry out the measurements. They also handed us an aluminum structure with functionality similar to the one needed for this project that was used in previous projects, so most of the components were reusable for the present system.

ETSEIB

- **Mechanical elements**

The mechanism consisted of two arms working as a fork attached to a shaft, with free rotation within supports with the help of ball bearings. However, as it was still not finished it lacked the right support and bearing and the correct fixing over a base. Table 3.1 and Figure 3.4 describe the different components of the construction.

Table 3.1*: Initial elements description*

Number	Element	Description
1	Support	Rectangular aluminum piece, used as support for the shaft. It has hole to insert the bearing.
2	Bearing	Deep groove ball bearing. d: D:
3	Base	Rectangular piece, used to fix both supports.
4	Shaft	Solid cylinder with free rotation on his longitudinal axis. It´s function is to transmit the motion from the actuator to the fork
5	Fork and wire fixing	The fork is formed by 2 equal pieces. It´s function is to fix the wire and do a curvilinear movement. The length, rigidity and inertia of this element are important parameters that must be taken into account in the study of viability.
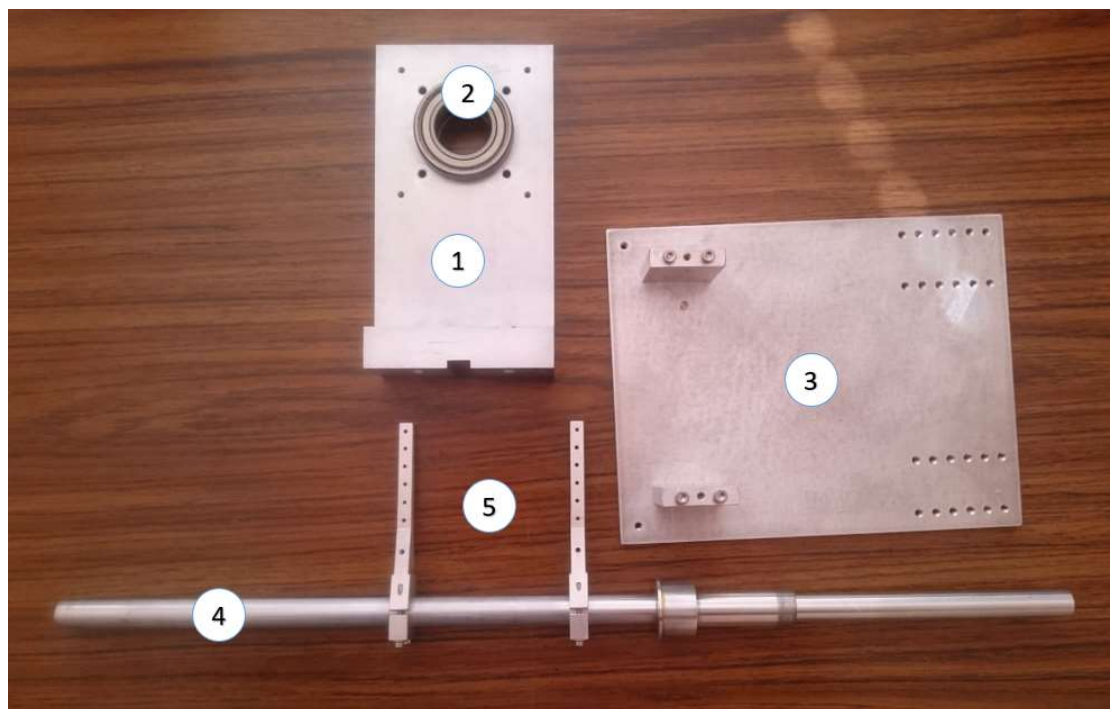
Figure 3.4*: Initial mechanical available elements*

ETSEIB

- **Electronic elements**

As it has been mentioned, we could dispose of some electronic devices from the mechanical department of the UPC. Those devices were:

- The **piezo actuator driver**, which includes an E-617.00F high-performance piezo amplifier (Figure 3.5) with a 230V-24V converter. These electronics modulate the signal to be readable for the piezo and also amplifies it with a gain factor of 10.

Figure 3.5: Piezo actuator driver board

- A **strain gauge + wire read out system**. This set is composed by a set of 4 Wheatstone bridges with a potentiometer in each channel. For the present project, only three channels will be used: two to measure the deformation of different strain gauge and a third one to measure the wire's deformation.
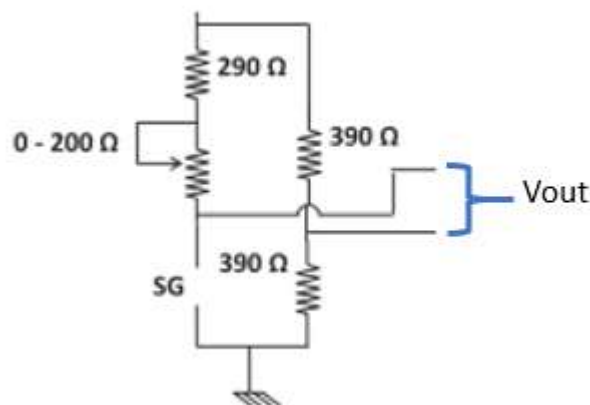
Figure 3.6: Strain gauge read out system's Wheatstone bridge

Notice that the potentiometer range is 200 ohms. This means that the gauges resistance value must be between 290 and 490 ohms.

A. The full circuit description with the resistances values is in the annex **"Strain gauge and wire read out system electronic circuit".**

- A **Picoscope** is an electronic device that, connected to a PC and with a software, works as an oscilloscope and signal generator at once. It will be used to produce the signal that is sent to the piezo as well as to read the signals from the strain gauges.

- **Piezoelectric actuator**

For the motion of the fork we use a low voltage piezoelectric actuator, in particular, the model P4821.20 of Physik Instrumente brand.

Figure 3.7: *From left to right, 60µm, 45µm, 30µm and 15µm stroke preloaded piezoelectric actuators*

The piezoelectric actuator is a small metal cylinder filled with small layers of a ceramic material (which is a piezoelectric material). This means that if we apply an electrical field to this material, it will suffer a deformation. This phenomenon, called piezoelectric effect, allows the conversion of electrical energy into mechanical energy.

Piezoelectric actuators (PZTs) offer several benefits and advantages over the other motion techniques:

- Nanometer and sub-nanometer sized steps at high frequency can be achieved.

They produce the motion through solid state crystal effects. There are no moving parts, so stick-slip effect is avoided.

- PZTs have an inverse proportional relation between the movement frequency and the load they are able to move. This means that they can move heavy loads at low frequencies but also can reach high frequencies like 10kHz with lighter loads.
- No maintenance is required because they are solid state and their motion is based on molecular effects inside the ferroelectric crystals.

Nevertheless, PZTs have an extremely short stroke. Specifically, the model that will be used has a maximum stroke of 30 µm, when the maximum allowable electric field is applied. For low voltage PZTs, this corresponds roughly to 100 volts.

ETSEIB

4. Study of possible mechanical solutions

Before starting the design of the wire scanner device, we need to study the viability of the different possible mechanisms. Though there are many potential possibilities, we are restricted by the characteristics of the piezoelectric actuator, limited to a linear movement with a tiny range of motion.

Given these constraints, it is clear that the original LHC wire scanner movement cannot be exactly reproduced, but with this study we aim to define whether there is a solution capable of offering acceleration and speed values high enough to obtain relevant vibration measurements.

4.1. Linear set up

Given the type of movement of the actuator, the first evident proposal is a linear wire scanner that cuts the beam profile in the direction of the piezoelectric motion. Some scanners are currently operating with this movement and the constructive solution would be pretty easy to design as we could directly move the wire with the actuator without needing any complex mechanism.

However, this set up has two important drawbacks that discard it as a viable option for our solution. The first one is that its mechanical behavior is really different from the one of the original LHC scanner. The wire dynamical equations would need to be completely overhauled and the obtained vibration results would be hard to scale to the real installation.

The other disadvantage is that with this configuration the maximum speed achieved by the wire cutting the beam would be pretty limited. The short travel range of the actuator does not leave much time for acceleration and the direct movement of the wire does not allow for any amplification.

4.2. Rotary set up

Having abandoned the linear configuration, the other logical solution is the one based on a rotary motion, which tries to mimic as closely as possible the actual scanner setup mounted in the LHC. The main advantage of this configuration is that the linear velocity that can be reached at the fork tips is much higher than in a linear set up, as the velocity is directly proportional to the distance to the axis of rotation.

With the available elements described in the previous section, those maximum reachable speeds will be probably far from those required for the new scanner. Anyway, we have

considered two potential mechanisms to implement a rotary system.

- **With amplification mechanism (flexors)**

The real scanner does a circular swept of 180 degrees. At first, the idea was to reproduce as close as possible that movement in our model. After some thought, and considering that the piezoelectric actuator has a 30 μm travel range, the conclusion was that this movement was far from being achievable. However, a bar mechanism could be used to amplify the fork tip displacement to try to reach the maximum possible amplitude.

One has to bear in mind that the travel range of the piezoelectric actuator is an order of magnitude smaller than the clearances of a classic mechanical joint, which are around 0,1 millimeters, so standard mechanisms have to be discarded. The solution that comes up is to use articulations without gaps: flexors. Flexors are mechanical elements that simulate the behaviour of a bar mechanism with the singularity that they do not have clearances, as they use the elastic properties of the materials to allow the movement.

Clearly, the advantage of this setup is that it allows the design of a mechanism formed by flexors that increases the range of the movement of the fork, thus replicating better the original wire scanner. Yet, the main drawback is that the maximum achievable acceleration and velocity would decay significantly as the range of movement is amplified, heavily affecting the system requirements. Furthermore, the design of the mechanism could be a heavy and difficult task that is not the main objective of this project. For all these reasons, this solution has been rejected.

- **Without amplification mechanism (direct application)**

As already said, the main difficulty of the model is trying to get the maximum range of movement at the fork tips, using the available piezoelectric actuator. Discarding the possibility of using a mechanism to amplify this range, the other option is to apply the piezoelectric force directly on a cam, adding a spring opposed to the actuator force, allowing the return movement (Figure 4.1).

ETSEIB
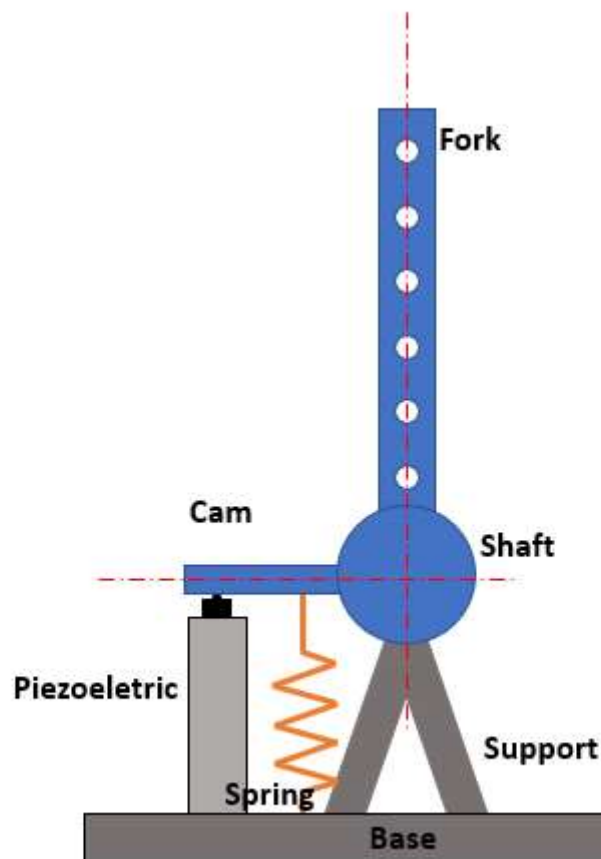
Figure 4.1: Direct application mechanism scheme

With this configuration, the range of movement loses importance in favour of other parameters like the acceleration or velocity. Even though the dimension of the movement will be lower, if the wire acceleration is close enough to the order of magnitude of the real scanner it will be possible to study the vibrations and deflections caused by that motion.

Using this type of setup, the barrier of the articulations clearances is eliminated as the shaft is constantly in direct contact with the actuator tip and moves along with it. Moreover, it is also a simple solution and fairly easy to build up, so it is clear that this will be the developed mechanical configuration.

4.3. Study of viability

The viability study requires the calculation of the maximum values of acceleration and velocity that the system with the piezoelectric actuator will be able to reach. As the purpose of this study is to just roughly estimate those maximum values, some simplifications have been assumed:

- The force application point of the spring and piezoelectric in the cam is considered at the same distance of the axis of rotation, with **e=0.**
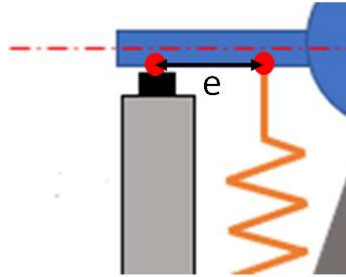
Figure 4.2: *Distance between piezo and spring*

- The spring force is considered to be constant as the spring elongation variation is minimal.
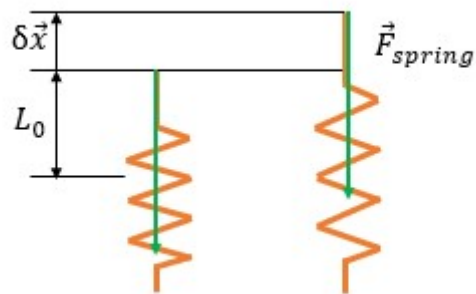
Figure 4.3: *Spring elongation*

$$\vec{F}_{spring} = -k \cdot (L_0 + \partial\vec{x}) \text{ with } \partial\vec{x} \lll \qquad \text{(Eq. 4.1)}$$

The system that has been chosen is simple, as is the equation obtained with this study taking the fork angular velocity $\dot{\theta}^*$ as a virtual velocity.

ETSEIB
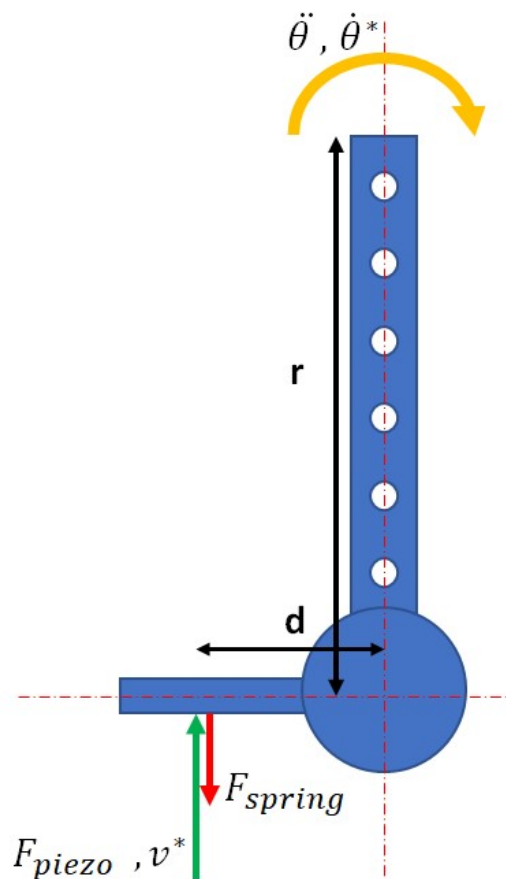
Figure 4.4: *Free body diagram*

$$F_{piezo} \cdot \dot{\theta}^* \cdot d - F_{spring} \cdot \dot{\theta}^* \cdot d - I \cdot \ddot{\theta} \cdot \dot{\theta}^* = 0 \qquad \text{(Eq. 4.2)}$$

Note that F_{piezo} and F_{spring} are arbitrarily decided within the limits of the piezoelectric characteristics and chosen spring, the distance d is constant as it just depends on the application point of the force of the piezo, and $\dot{\theta}^*$ can be eliminated.[6] Thus, the equation depends just on the angular acceleration $\ddot{\theta}$ and the inertia of the moving parts I.

So, doing a fine estimation of the rotating elements inertia, the value of the maximum achievable acceleration will be obtained. For this purpose, the pieces (which will be explained on chapter 6.1) are built using a CAD program which calculates the inertia of the parts with respect to their axis of rotation.
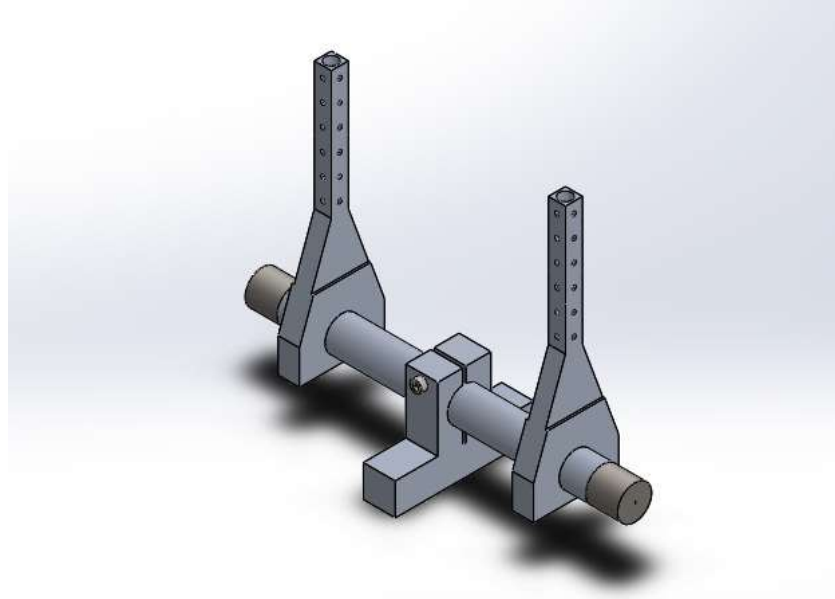
Figure 4.5: Moving parts assembly

Software output: **Ixx** =15027 $g \cdot mm^2$=15027 $kg \cdot m^2$

It is easy to isolate the acceleration term from **Eq. 4.2**:

$$\ddot{\theta}_{max} = \frac{(F_{piezo} - F_{spring}) \cdot d}{I} \qquad \text{(Eq. 4.3)}$$

With the value of the maximum possible acceleration and considering that the phases of acceleration/deceleration are constantly at their peak (Figure 4.6), the linear velocity of the fork at the phase of constant speed can be obtained through**:**

$$\theta_1 = \frac{1}{2} \cdot \ddot{\theta} \cdot T^2 \qquad \text{(Eq. 4.4)}$$

$$\dot{\theta}_{ct} = \ddot{\theta} \cdot T \qquad \text{(Eq. 4.5)}$$

$$v_{ct} = \dot{\theta}_{ct} \cdot r \qquad \text{(Eq. 4.6)}$$

where T is the time required to travel from rest to θ_1.

ETSEIB
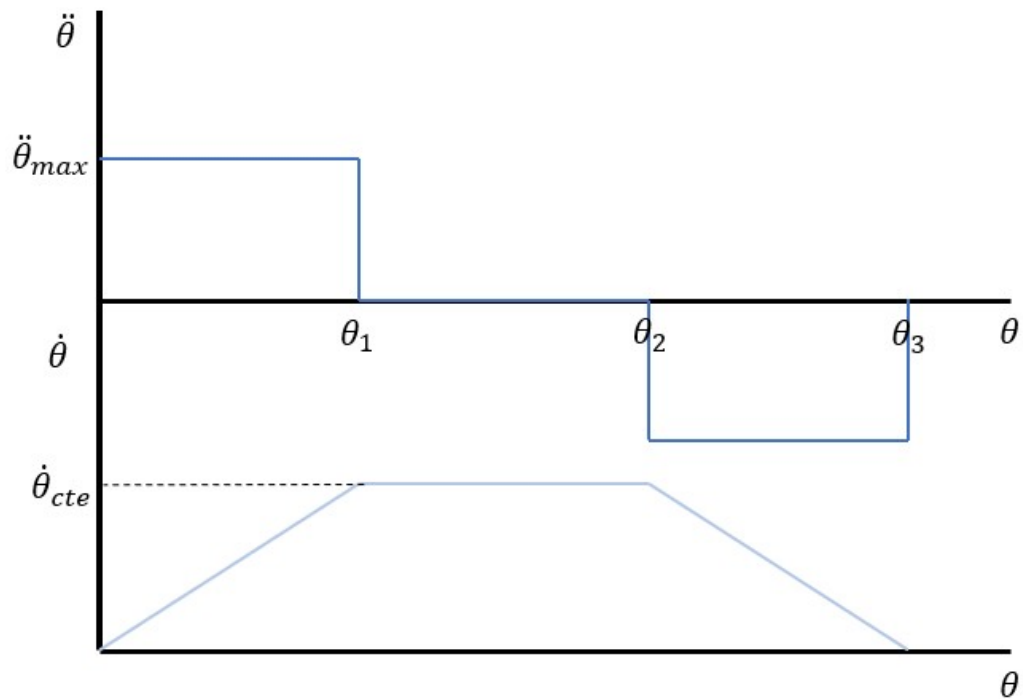
Figure 4.6: Ideal behavior of the angular velocity and acceleration

Although it has been considered that the acceleration curve has a discrete behaviour with instantaneous change of value, this is supposing an ideal situation. In the real system this is not physically possible, so the values obtained are always higher than the real ones. However, they give an idea of the limits that we are bound to.

At this point, in order to carry out these estimations the only parameter left to be fixed is the angle θ_1 swept during the acceleration phase. For this, first we need to calculate the total available angle allowed by the geometry and the actuator travel range:
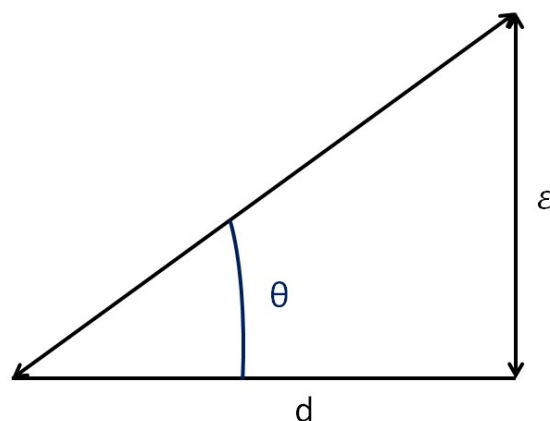
Figure 4.7: Available angle

As we want as much rotation as possible, we decide to establish d=1mm, considering it to be the closest distance between the point of force application and the shaft axis to be reliable to build. Knowing also that the piezoelectric travel range is of 30 µm(Ɛ), the total available angle is:

$$\theta_{total} = \arctan\left(\frac{\varepsilon}{d}\right) = \arctan\left(\frac{0,03}{1}\right) = 1,71835° = 0,03 \; rad \quad \textbf{\textit{(Eq. 4.7)}}$$

For these estimations, we consider to split the rotation equally between the three phases, resulting in:

$$\theta_1 = \theta_2 - \theta_1 = \theta_3 - \theta_2 = \frac{\theta_{total}}{3} = 0,5728° = 0,01 \; rad \qquad \textbf{\textit{(Eq. 4.8)}}$$

With all this, using equations 4.3, 4.4, 4.5 and 4.6 and defining $F_{piezo} = 1000 \; N$ and $F_{spring} = 500 \; N$, the estimations result in:

Table 4.1: *Estimations results*

θ_{total}	$0,03 \; rad$
θ_1	$0,01 \; rad$
T	$3,47 \; ms$
$\ddot{\theta}_{max}$	$3327,3 \; rad/s^2$
$\dot{\theta}_{ct}$	$5,76 \; rad/s$
v_{ct}	$0,5767 \; m/s$

The analysis of these results shows that the proposed system performance is far from achieving the requirements of the original wire scanner, which demands a constant cutting speed of around 20 m/s. The main factor for this failure is the tiny travel range of the piezoelectric actuator, which restricts the rotation to less than 2º and limits the acceleration time, thus restraining the attainable speed.

Nevertheless, the maximum acceleration value has the same order of magnitude as the original LHC scanner. This allows us to continue with this set up and try to study its behaviour, as the acceleration is the main cause of the wire vibration and therefore some of the obtained

results could be useful for the understanding of the real original system.

Furthermore, these are only mere estimations and the adjustment of some of the parameters (such as the spring force or the distribution of the available angle between the three phases) can lead to better results. For these reasons, we are positive about accepting this mechanism as a viable solution.

5. Dynamics

In order to facilitate the mechanical study of the wire vibrations, Juan Herranz **[1]** defined a simplified model for the scanner mechanism and characterized the dynamics of the carbon wire. In this project we will use the exact same parameterization that he presented, so this chapter intends just to resume his work for a proper understanding of the system.

5.1. Model of the wire scanner

The wire scanner mechanism model is shown in Figure 5.1. The fork is modelled as two rigid bars of length H, which follow exactly the shaft rotation movement $\theta(t)$. The tips of the left and right fork arms are called A and B and their distance to the middle point of the shaft is L_0.
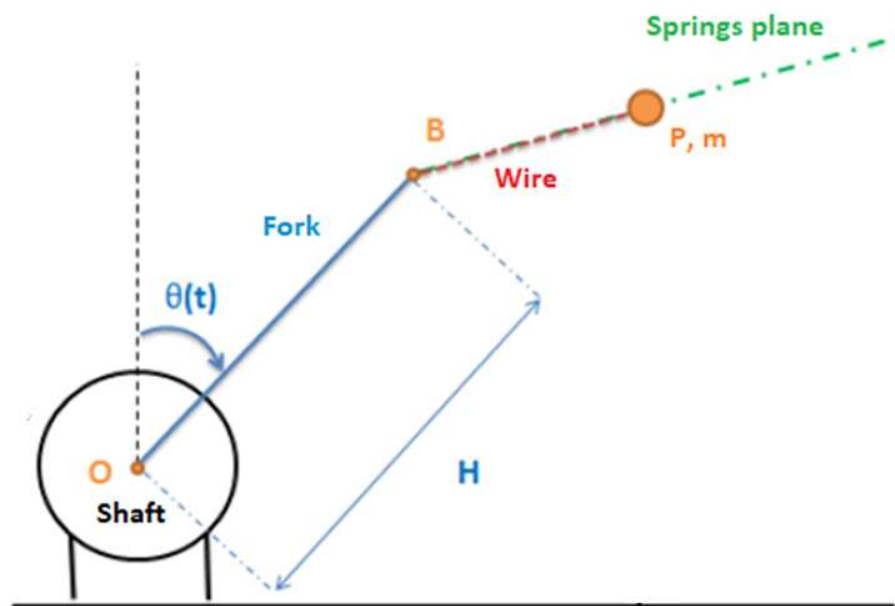
Figure 5.1: Mechanism and wire model scheme

The carbon wire is located between the tips A and B and, although in reality it is a continuous solid, we model it as two equal springs of constant k with a singular mass m on their point of attachment P.

We are assuming that there is a complete symmetry between the two fork arms; therefore, the singular mass does not vary its longitudinal position along the wire. With this consideration, there is always a plane perpendicular to the shaft axis containing A, B and P, which is referred as the springs plane (Figure 5.2).
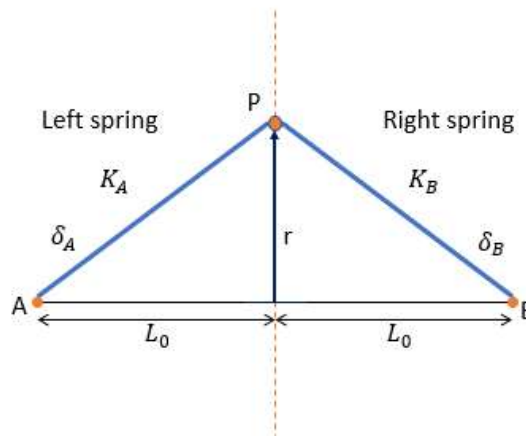
Figure 5.2: Springs plane. Wire modeled as 2 symmetric springs

The movement of the point P relative to the fork has 2 degrees of freedom that can be expressed with the following Cartesian coordinate system (Figure 5.3):

- x is perpendicular to the plane defined by the fork arms.
- y is coincident with the longitudinal axis of the fork.

In order to study the wire vibrations, we need the total displacement of point P, which is referred as $r = \sqrt{x^2 + y^2}$.
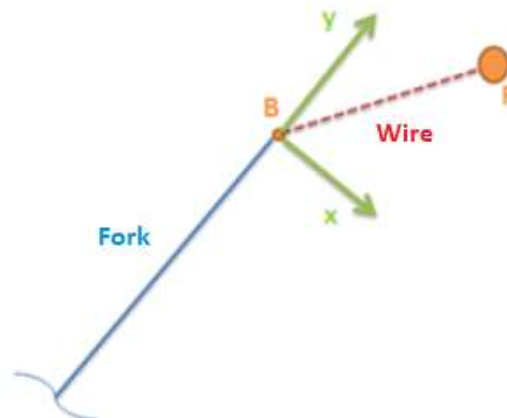
Figure 5.3: Coordinate system

The origin of the coordinate system is placed in the middle point of the segment AB and it moves together with the fork with the single forced degree of movement $\theta(t)$.

ETSEIB

5.2. Wire dynamic equations

Using the wire scanner model, studying the dynamics of the wire translates into defining the movement equation of point P, which contains the singular mass m. This movement equation will allow us to obtain the wire behaviour under all possible forced stimulations by the actuator.

The movement equation is obtained using Newton's 2nd law in a Galilean reference (the ground G), which nullifies the inertia and Coriolis forces and simplifies as:

$$\sum \bar{F}(P) = m \cdot \overline{a_G}(P) \qquad (Eq.\ 5.1)$$

All calculus are made using vector base B (Figure 5.4), which is defined in the same way as the aforementioned coordinate system but with its origin displaced longitudinally to the axis of the shaft, on point O. This change is made to facilitate the definition of the dynamic vectors, as the only forced movement $\theta(t)$ has its centre of rotation on this same axis.
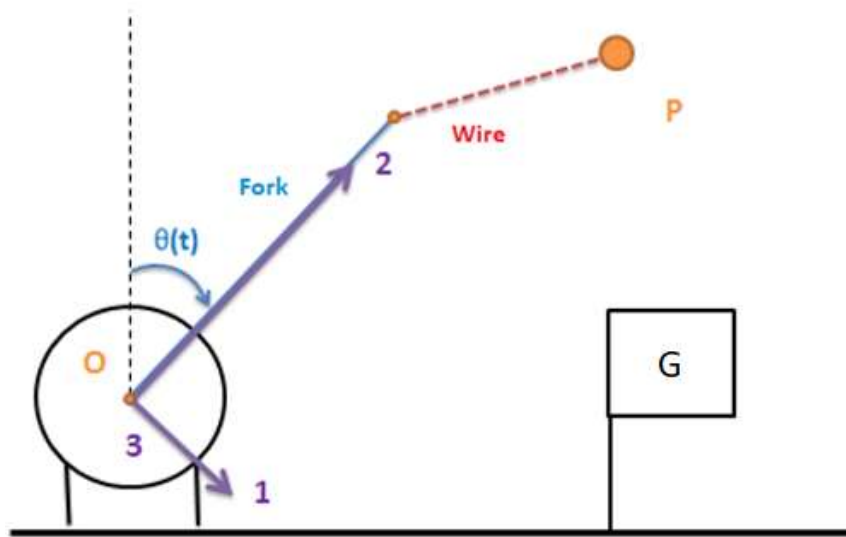
Figure 5.4: Vector base B

To obtain the acceleration $\overline{a_G}(P)$ we need to get the position vector $\overline{OP}$ in the base B and derive it, also taking into account the rotation of the base $\overline{\Omega}_G^B$:

$$\{\overline{v_G}(P)\}_B = \frac{d}{dt}\{\overline{OP}\}_B + \left\{\overline{\Omega}_G^{B}{}^{\overline{OP}}\right\}_B \qquad (Eq.\ 5.2)$$

$$\{\overline{a_G}(P)\}_B = \frac{d}{dt}\{\overline{v_G}(P)\}_B + \left\{\overline{\Omega}_G^{B}{}^{\overline{v_G}(P)}\right\}_B \qquad (Eq.\ 5.3)$$

ETSEIB

Applying this expression with the defined coordinate system and taking $\overline{\Omega}_G^B = \dot{\theta}(t)$:

$$\{\overline{OP}\}_B = \left\{ \begin{matrix} x \\ H + y \end{matrix} \right\}_B \qquad \text{(Eq. 5.4)}$$

$$\{\overline{v_G}(P)\}_B = \left\{ \begin{matrix} \dot{x} + \dot{\theta}(t) \cdot (H + y) \\ \dot{y} - \dot{\theta}(t) \cdot x \end{matrix} \right\}_B \qquad \text{(Eq. 5.5)}$$

$$\{\overline{a_G}(P)\}_B = \left\{ \begin{matrix} \ddot{x} + \ddot{\theta}(t) \cdot (H + y) + 2\dot{y}\dot{\theta}(t) - \dot{\theta}^2(t) \cdot x \\ \ddot{y} - \ddot{\theta}(t) \cdot x - 2\dot{x}\dot{\theta}(t) - \dot{\theta}^2(t) \cdot (H + y) \end{matrix} \right\}_B \qquad \text{(Eq. 5.6)}$$

The interaction forces acting on the P particle are mainly the springs forces. The wire weight is much lower than those forces and will be neglected.

It has been considered that the spring forces are attractive because, in a resting position, the wire is stretched between the fork tips with a tension F_0. Assuming that the springs are linear with k as elastic constant, the spring force is given by the following expression:

$$F_s = F_0 + k \cdot \Delta\delta \qquad \text{(Eq. 5.7)}$$

where $\Delta\delta$ represents the length increase of the springs with respect to the initial spring length in the resting situation.

Figures 5.5 and 5.6 show those forces (on the springs plane) and their values.
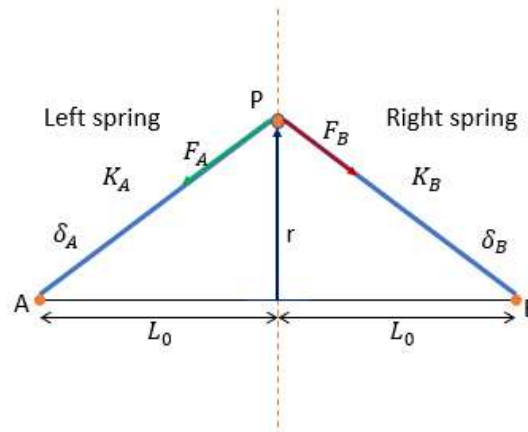
Figure 5.5: Forces on particle P
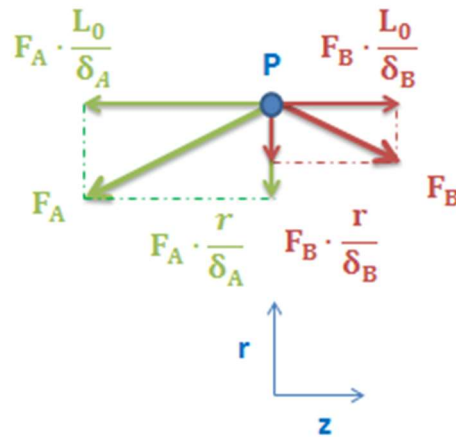
Figure 5.6: Forces projection on the radial (r) and longitudinal (z) directions

where:

$$F_A = F_0 + k \cdot \left[\sqrt{x^2 + y^2 + L_0{}^2} - L_0 \right] \qquad (Eq.\ 5.8)$$

$$F_B = F_0 + k \cdot \left[\sqrt{x^2 + y^2 + L_0{}^2} - L_0 \right] \qquad (Eq.\ 5.9)$$

The springs forces can be projected on the z and the r directions. Figure 5.7 shows the forces projected on the plane x-y:
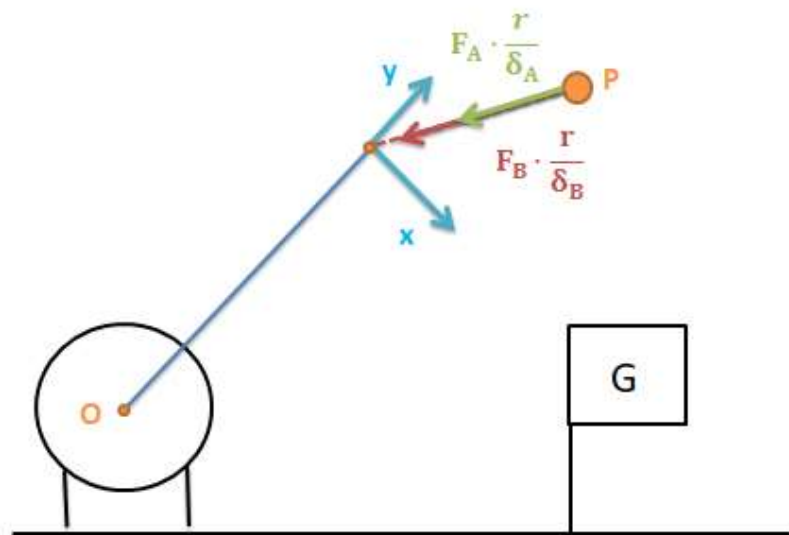
Figure 5.7: Forces diagram on x-y plane

The projection of the forces in the vector basis B is:

$$\sum \bar{F}(P) = \begin{cases} -\left(\frac{F_A}{\delta_A} + \frac{F_B}{\delta_B}\right) \cdot x \\ -\left(\frac{F_A}{\delta_A} + \frac{F_B}{\delta_B}\right) \cdot y \end{cases}_B \qquad \text{(Eq. 5.10)}$$

Finally, combining Eq. 5.8, Eq. 5.9 and Eq. 5.10, the equations of motion for particle P are:

$$\begin{cases} -\left(\frac{F_A}{\delta_A} + \frac{F_B}{\delta_B}\right) \cdot x \\ -\left(\frac{F_A}{\delta_A} + \frac{F_B}{\delta_B}\right) \cdot y \end{cases}_B = m \cdot \begin{cases} \ddot{x} + \ddot{\theta}(t) \cdot (H + y) + 2\dot{y}\dot{\theta}(t) - \dot{\theta}^2(t) \cdot x \\ \ddot{y} - \ddot{\theta}(t) \cdot x - 2\dot{x}\dot{\theta}(t) - \dot{\theta}^2(t) \cdot (H + y) \end{cases}_B \qquad \text{(Eq. 5.11)}$$

As the spring forces F_A and F_B depend of the second order terms of the coordinates (x,y) the system is nonlinear, and that hinders its analysis and posterior simulations. Assuming that the range of the wire displacements is much lower than its total length, it is safe to consider a small vibrations scenario around its equilibrium configuration (0,0,0).

Assuming $\frac{x}{L_0}, \frac{y}{L_0} \ll 1$, 2nd order terms can be simplified. Applying Taylor expansion, the equations of motion simplify to:

$$\begin{cases} -\frac{2F_0}{L_0} \cdot x \\ -\frac{2F_0}{L_0} \cdot y \end{cases}_B = m \cdot \begin{cases} \ddot{x} + \ddot{\theta}(t) \cdot (H + y) + 2\dot{y}\dot{\theta}(t) - \dot{\theta}^2(t) \cdot x \\ \ddot{y} - \ddot{\theta}(t) \cdot x - 2\dot{x}\dot{\theta}(t) - \dot{\theta}^2(t) \cdot (H + y) \end{cases}_B \qquad \text{(Eq. 5.12)}$$

5.3. Fork rotational motion pattern

Once the wire dynamics have been modelled, its behaviour under any motion of the fork driven by the actuator can be predicted.

The next step is to find a motion pattern that fulfils the same constraints as the one of the LHC scanner fork while minimizing the wire vibrations. The physical restrictions of the system (particularly, the actuator limitations) have to be taken into account, as it needs to be implemented in the experimental prototype.

The motion pattern will be defined through the angular acceleration curve, which then will be integrated to obtain the angular speed and travelled angle. That acceleration curve has to:

- Contain the three motion phases of the scanner: acceleration, constant speed and deceleration.
- Have smooth transitions between the phases. Additionally, sharp edges on the curve have to be avoided as they would add more vibrations, which is the opposite goal of this project.

- • Be bounded by the limitations of the mechanical system, as estimated in Table. 4.1.

Our first choice for the angular acceleration curve is an inverted cosine with an amplitude of $a = \frac{\ddot{\theta}_{max}}{2}$ in the first phase, a constant null second phase and a third phase equal to the first one but with opposite sign:

Table 5.1: Angular acceleration equations

	$t \leq T$	$\ddot{\theta}_1(t) = a\left(1 - \cos\left(\frac{2\pi t}{T}\right)\right)$
$\ddot{\theta}(t)$	$T \leq t \leq 2T$	$\ddot{\theta}_2 = 0$
	$2T \leq t \leq 3T$	$\ddot{\theta}_3(t) = -a\left(1 - \cos\left(\frac{2\pi t}{T}\right)\right)$

The values estimated in Table 4.1 ($\ddot{\theta}_{max} = 3327\ rad/s^2$ and $T = 3{,}47\ ms$) yield (Figure 5.8):
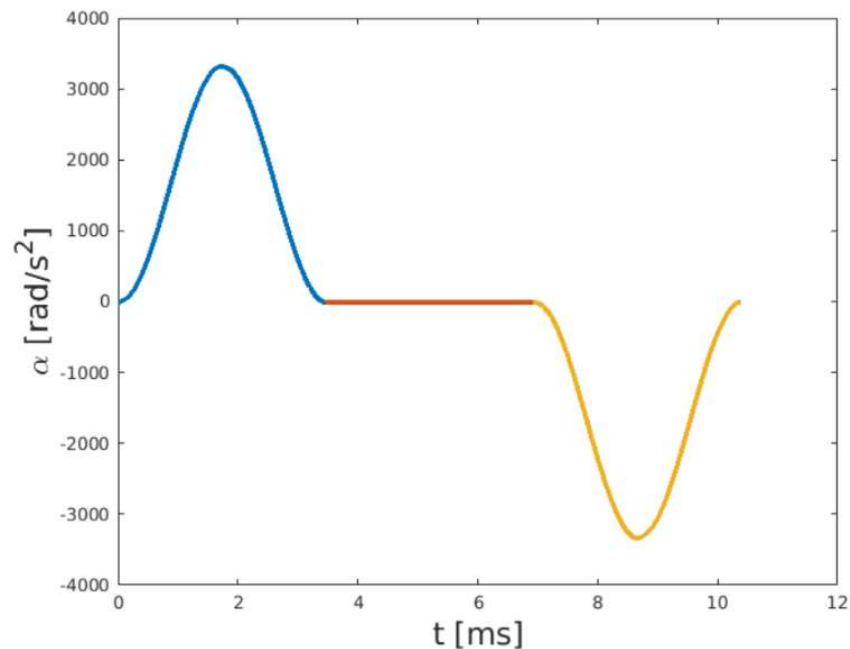
Figure 5.8: *Angular acceleration*

The first time derivative of the acceleration yields the angular speed (Table 5.2 and Figure 5.9):

Table 5.2: Angular speed equations

$\dot{\theta}(t)$	$t \leq T$	$\dot{\theta}_1(t) = a\left(t - \dfrac{T}{2\pi}\sin\left(\dfrac{2\pi t}{T}\right)\right)$
	$T \leq t \leq 2T$	$\dot{\theta}_2 = aT$
	$2T \leq t \leq 3T$	$\dot{\theta}_3(t) = 3aT - a\left(t - \dfrac{T}{2\pi}\sin\left(\dfrac{2\pi t}{T}\right)\right)$
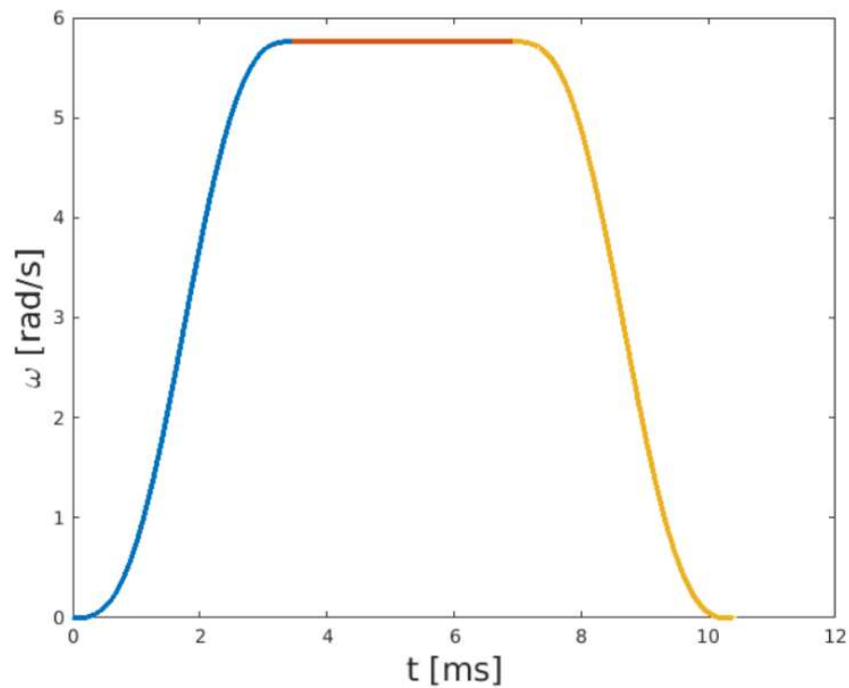
Figure 5.9: Angular speed

A second time derivative yields the travelled angle (Table 5.3 and Figure 5.10):

***Table 5.3**: Travelled angle equations*

$\theta(t)$	$t \leq T$	$\theta_1(t) = \left(\frac{a}{2}\right)\left(t^2 + \frac{T^2}{2\pi^2}\right)\left(\cos\left(\frac{2\pi t}{T}\right) - 1\right)$
	$T \leq t \leq 2T$	$\theta_2(t) = \theta_1 + aT(t - T)$
	$2T \leq t \leq 3T$	$\theta_3(t) = \theta_2 + aT(t - 2T) - \left(\frac{a}{2}\right)\left((t - 2T)^2 + \frac{T^2}{2\pi^2}\right)\left(\cos\left(\frac{2\pi(t - 2T)}{T}\right) - 1\right)$
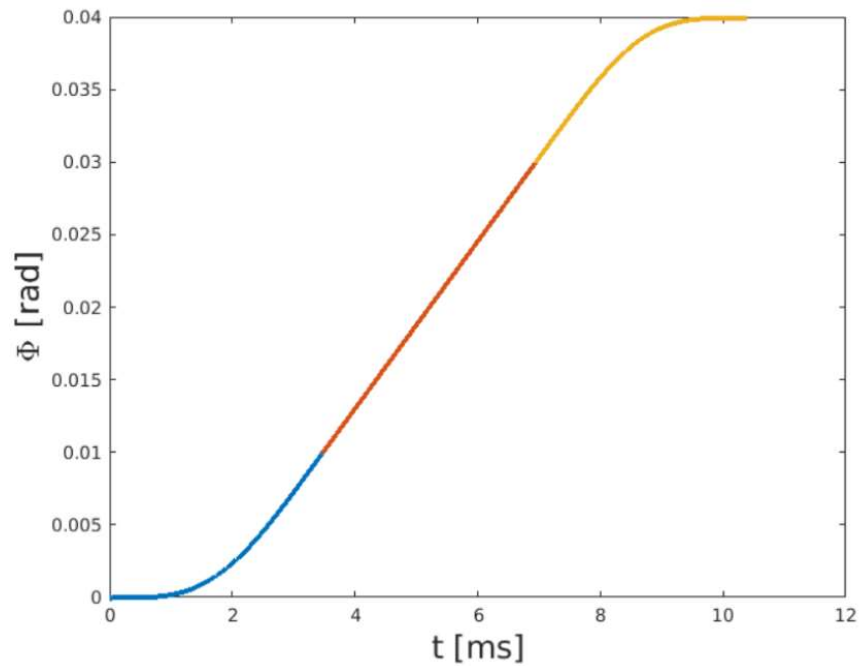
***Figure 5.10**: Travelled angle*

5.4. Wire scanner simulation

Before applying then designed fork motion pattern to the wire scanner prototype it is useful to carry out a mathematic simulation that help us predicting its behaviour and check if the real system works close to the model. The differential equation system to resolve is the Eq. 5.12.

Where $\ddot{\theta}(t)$ and $\dot{\theta}(t)$ correspond to the acceleration and speed curves of the fork motion pattern (Table 5.1 and Table 5.2). The meaning of the constant parameters and their value

considered for the simulation is:

- Initial tension of the springs: $F_0 = 0,1 \, N$
- Initial length of the springs: $L_0 = \frac{L_{wire}}{2} = 0,05 \, m$
- Wire mass: $m = 1,67 \cdot 10^{-7} \, Kg$
- Length of the fork arms: $H = 0,1 \, m$

Note that the F_0 and m values are taken from the original wire of the LHC Scanner and are really hard to adjust and measure in our prototype. This means that the results of this simulation could differ significantly from the measured ones in terms of absolute values, although the general behavior and shape of the displacement curves should be pretty similar.

Solving the differential equation system (Eq.5.12), the behavior of variables x and y is shown in Figure 5.11 and Figure 5.12. A 4th phase has been added after the deceleration in order to see the free vibration of the wire once it stops. Figure 5.13 represents the absolute displacement of the P particle as $r = \sqrt{x^2 + y^2}$.
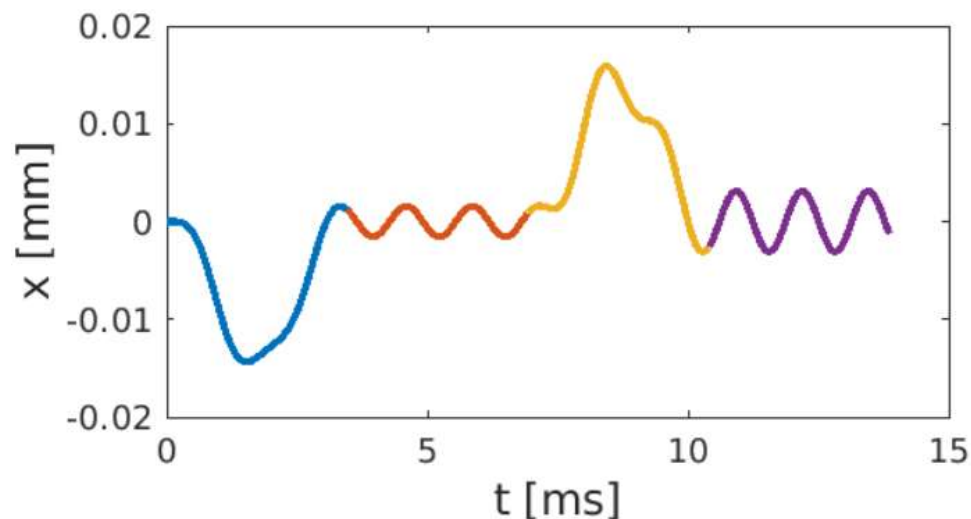
Figure 5.11: x component

The x component corresponds to the displacement of the wire tangential to the rotational circle fork tips it is mostly function of the angular acceleration $\ddot{\theta}(t)$. Figure 5.12 shows that its behaviour is almost a complete inversion of the acceleration curve and it reaches relevant displacement values of more than 0.01 mm. The oscillation around 0 during the constant speed phase corresponds to the free vibration of the wire, as it does in the final rest.
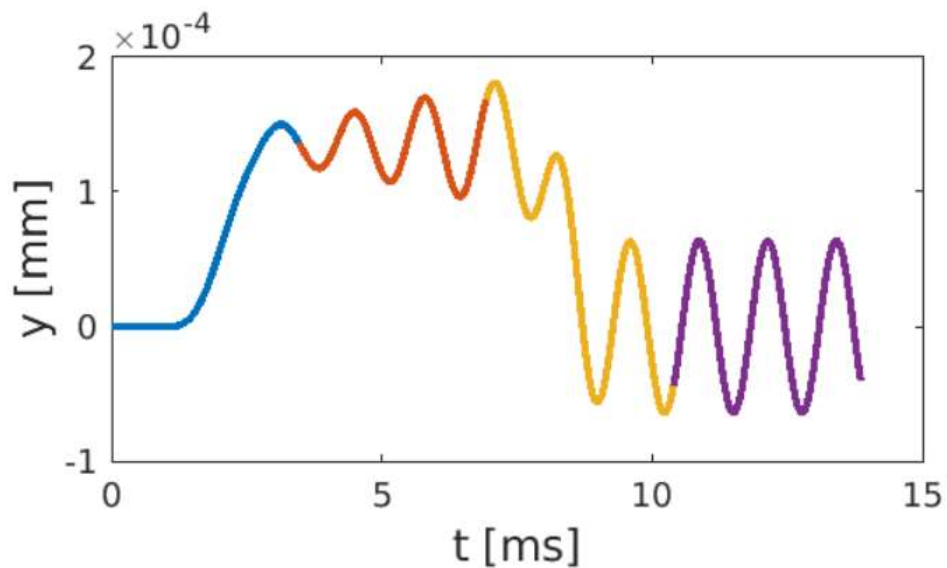
Figure 5.12: y component

On the other hand, as the y component corresponds wire displacement in the direction of the fork axis it is mostly function of the square of the angular speed $\dot{\theta}^2(t)$. On Figure 5.13 we observe that it begins to increase in the middle of the acceleration phase, as the square of the speed is negligible for low speed values. Then it oscillates around a constant value during the constant speed phase and around 0 in the final rest. Note that its displacement values are almost negligible against the x component.

Figure 5.13 represents the absolute displacement of the P particle as $r = \sqrt{x^2 + y^2}$ and figure 5.14 the wire length increase as $\Delta\delta = 2 \cdot \left[\sqrt{x^2 + y^2 + {L_0}^2} - L_0 \right]$.
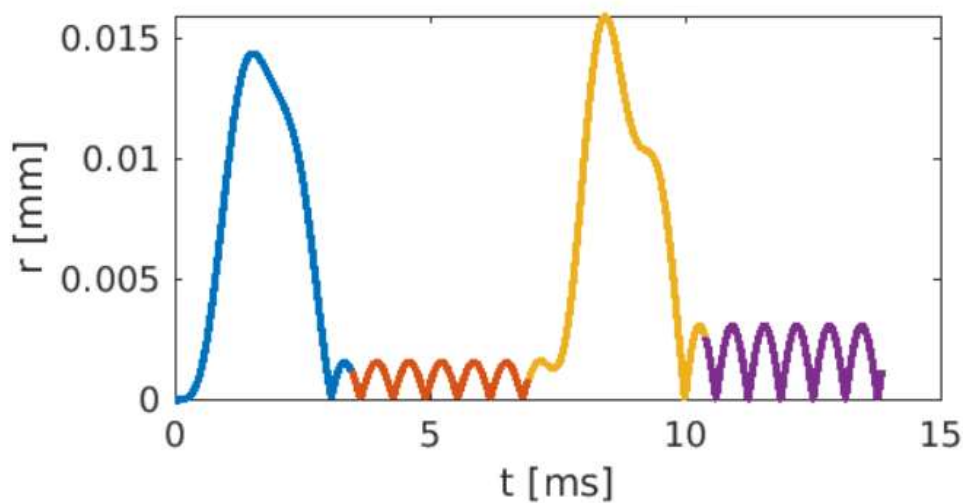
Figure 5.13: absolute displacement r

Absolute displacement of the virtual particle P is almost identical to the x component with only positive values, as we have seen that the y component has irrelevant influence. Note that the frequency of the free oscillations is the double, as the absolute character of the wave transforms a full positive and negative cycle into 2 positive ones.
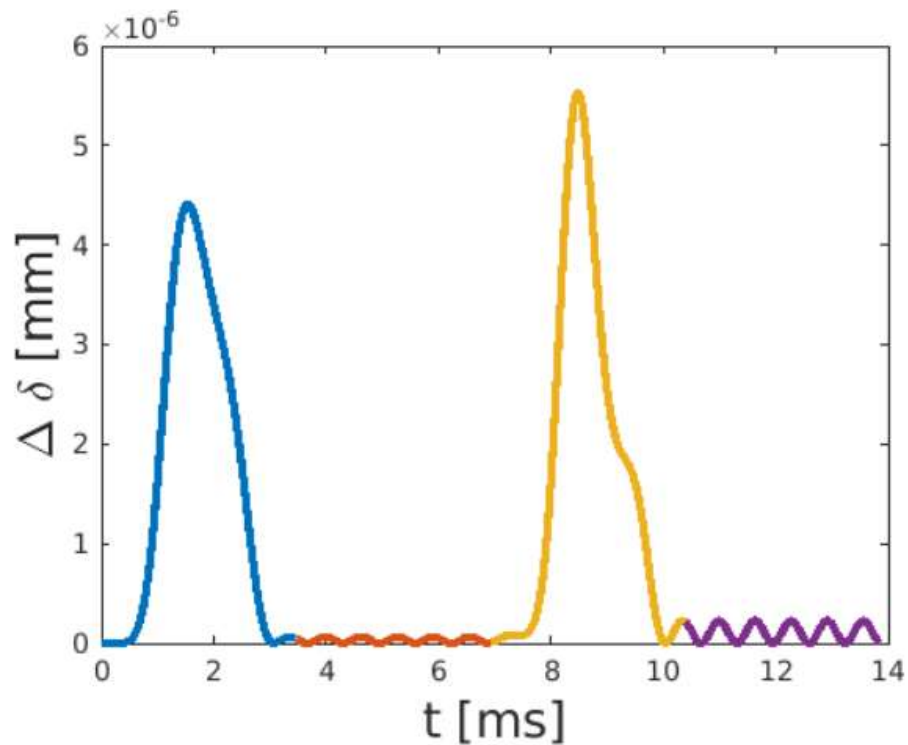
Figure 5.14: wire elongation

Finally, the length increase behavior is pretty much the same as the absolute displacement r, although the magnitude order is around 1000 times less. This is explained because in its definition $\Delta\delta = 2 \cdot \left[\sqrt{x^2 + y^2 + {L_0}^2} - L_0\right]$, the x and y values are much smaller than the original length of the wire springs L_0, thus the variations in the wire position represent a pretty little increase of its length.

6. Mechanism design and assembly

Once the most significant aspects of the mechanical system have been defined, the pieces have to be designed and manufactured. For this purpose, we have built a model in Solidworks (a 3D CAD program). Even though the design is completely defined, there are some specifications for the pieces. Through this chapter we will explain the design of the pieces as well as the normalized elements that have been used, and the full assembly of the mechanism.

The following image (Figure 6.1) shows an assembly of the mechanism that has been designed. Along the chapter 6.1 and 6.2 all the parts of the assembly will be explained but is good to have a previous idea of the mechanism to understand the job of each piece.
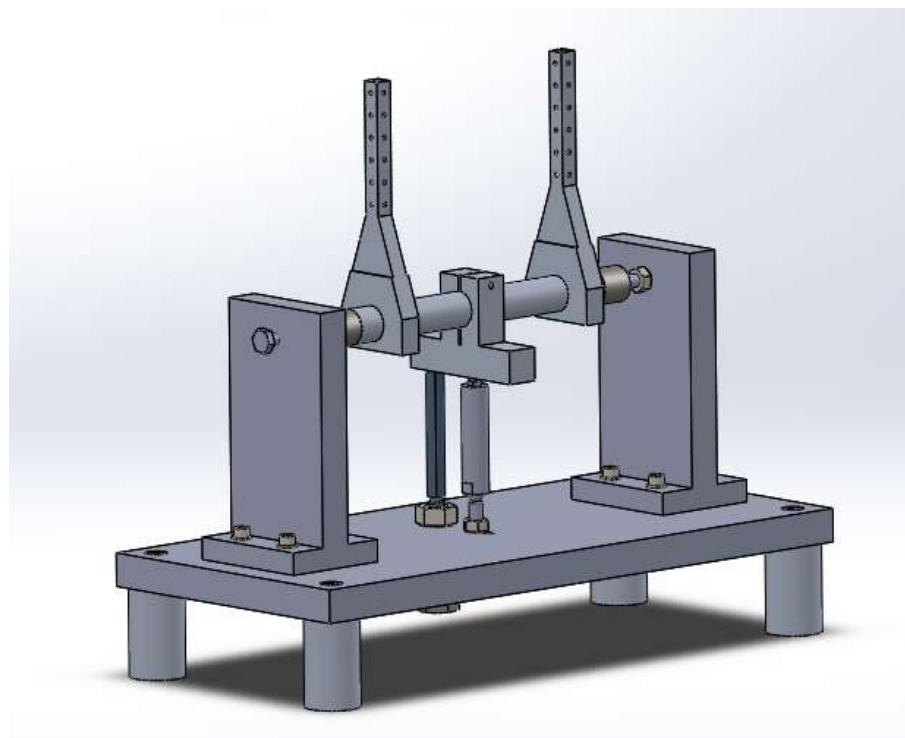
Figure 6.1*: Mechanism 3D CAD*

As described in chapter 4.2, the basic operation of the mechanism consists of a linear actuator displaced a distance from the centre, which causes the shaft and fork to rotate a certain angle. The mechanism returns to its initial position when the actuator does, with the help of a compression spring.

6.1. Parts

- **Designed parts**

The manufacturing process used to obtain all the new pieces has been CNC machining. Starting from either a block or a cylinder, the excess material is eliminated until the shape is that of the final piece.

- Shaft

The shaft is an aluminium cylinder which has its extremes mechanized Its diameter decreases linearly from 16mm to 8mm, where a hardened cap is fitted.
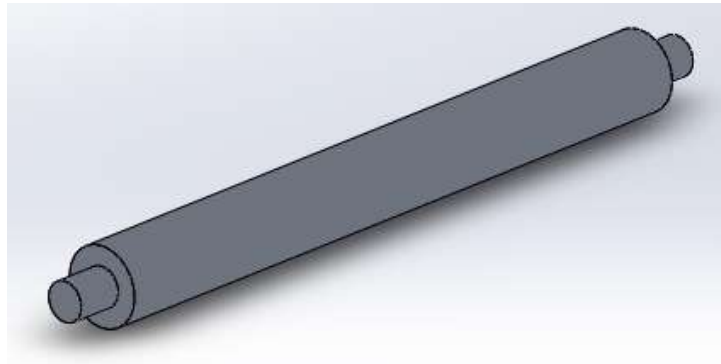
Figure 6.2: Shaft CAD

The shaft´s purpose is to hold the forks and transmit the force from the cam to the forks. Moreover, it is the link between the moving parts and the fixed parts (supports and screws, respectively) through the hardened cap.

- Base

The base is an aluminium rectangle of 300mm x 140mm x 10mm.
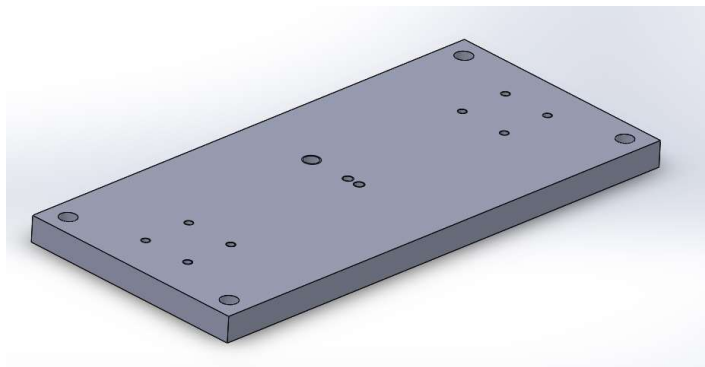
Figure 6.3: Base CAD

The two supports of the shaft are fixed on that base. The base has also the threaded holes to introduce the piezo and the springs screws, which will allow the assembling and adjustment of both parts.

Initially, the base had just one threaded hole 1mm away from the centre of the piece for the positioning of the piezo. However, after a few tests, we found that 1mm was too short a distance to transmit the force of the piezo to the shaft. The conclusion was that we needed to mechanize another hole 9mm away from the centre of the piece. Thus, the problem is fixed but the angle swept by the fork is reduced.

The base has also 4 threaded holes to fix the foots.

- Cam

The cam is an aluminium part that is fixed to the middle point of the shaft by tighten a screw.
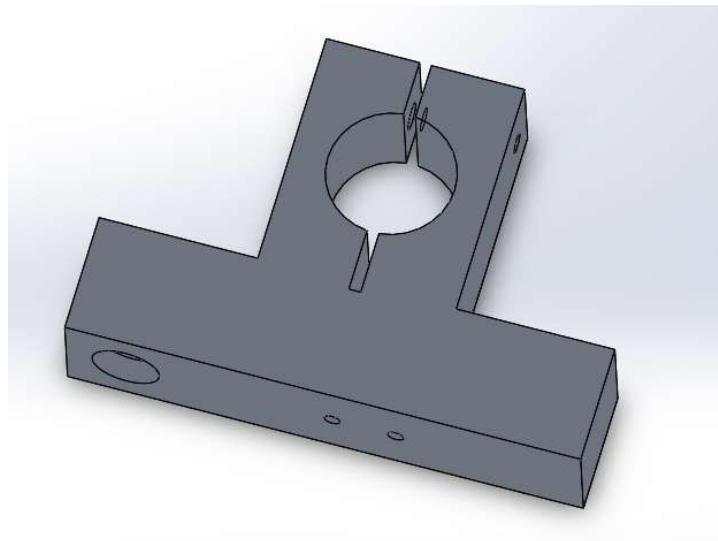
Figure 6.4: Cam CAD

As with the base, initially the cam had only one hole for the piezo 1mm away from the centre of the cam, and another one to house the end of the spring. After a few tests, where we changed the position of the piezo in the base, we decided to do another hole 9mm away from the centre of the cam, so that the piezo could be aligned vertically.

- Foot

The feet are 4 aluminium cylinders, each one fixed to the base through a screw. The role of the foots is to lift the base from the ground to free up the access to the piezo and spring´s

ETSEIB

adjustable screws.
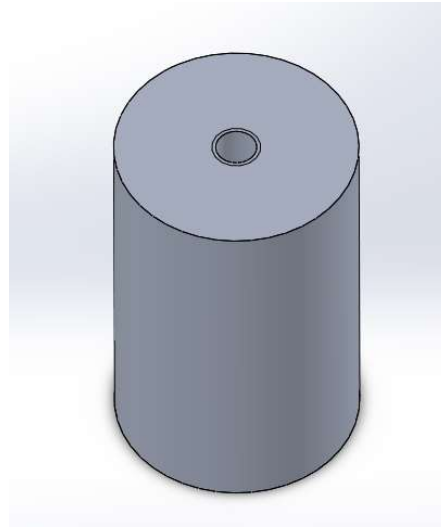
Figure 6.5: Foot CAD

- Hardened Cap

This piece is a small holed cylinder that is fitted to the shaft ends. It is made with F-125 steel. This particular choice of steel has been made because it the cap has to be in contact with the screws, which are made of high hardness steel. The F-125 steel is a high strength alloy steel with applications to parts of not very high thicknesses, that may support great fatigue efforts, admits induction hardening and welding. Another advantage is that it is good for mechanize. Thus, both parts have nearly the same hardness and we prevent the deformation of the shaft and ensure the correct contact between the screw and the cap.
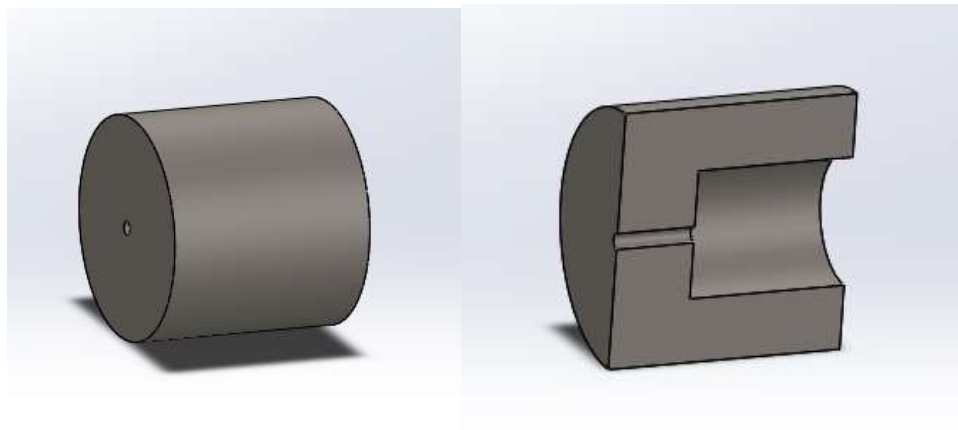
Figure 6.6: Hardened cap CAD

The cap has a passing hole of 1mm of diameter where the screw tip is introduced.

In order to fit the cap to the shaft, there is an interference fit. For forced unions, with hammer assembly, it is recommended to use H7-k6, as it is specified in the UNE-EN ISO 286-1:2011 **[5]** norm. For our pieces, we consider that it is not necessary an IT6 quality for the shaft, so we have assigned an IT7, while the union is left as H7-k7. The specification of the norm can be seen in Table 6.1 (extracted from the norm).

Table 6.1*: Recommended fits ISO*

Single hole		Seat features
H8 H8	x8 u8	Hard pressed. Press assembly.
H7	s6	Pressed. Press assembly.
H7	r6	Light pressed
H7	n6	Very forced. Hammer mount.
H7	k6	Forced. Hammer mount.
H7	**j6**	**Light forced. Mace mounted.**
H7	h6	Sliding with lubrication
H8	h9	Sliding without lubrication
H11	h9	Sliding
H11	h11	Sliding

- <u>ISO 4017 M6 30º Mechanized</u>

The screw is mechanized starting from a metric 6 ISO 4017 one. The final screw has a

conic form with a pointed ending (Figure 6.7).
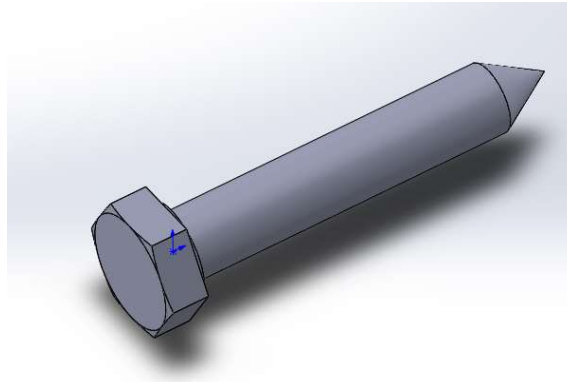
Figure 6.7: ISO 4017 M6 30° Mechanized CAD

- ISO 4017 M6 Piezo Mechanized:

Starting from the same type of screw, metric 6 ISO 4017, a hole of Ø3mm is mechanized at the threated end (Figure 6.8).
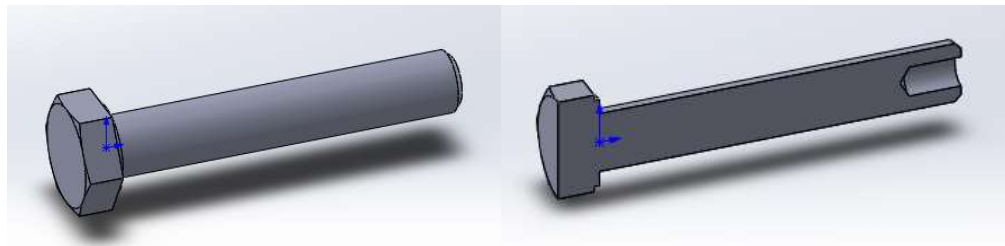
Figure 6.8: ISO 4017 M6 Piezo Mechanized CAD

- ISO 4017 M10 Spring Mechanized

The starting point is a metric 10 ISO 4017 screw. The diameter is decreased, and the

thread is removed (Figure 6.9).
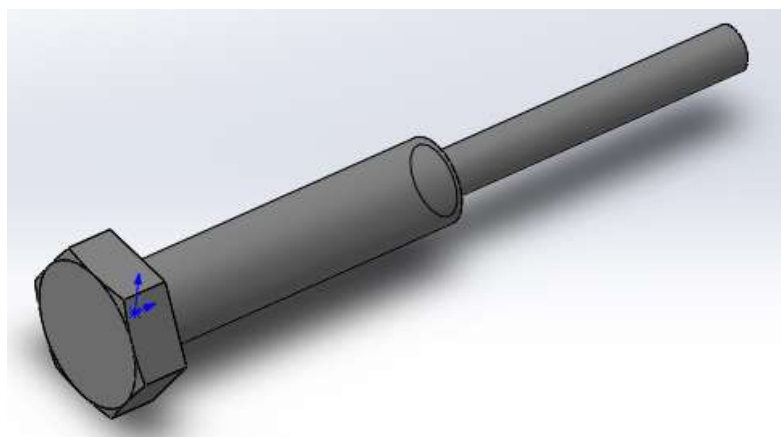
Figure 6.9: ISO 4017 M6 Spring Mechanized CAD

- Support:

The support is a T-shaped aluminium piece (Figure 6.10). It is mechanized with 4 threaded through holes in the base and another one on the top side of the piece. This last hole is intended to house the screw with a 30º mechanized tip, which holds the shaft and the forks together.
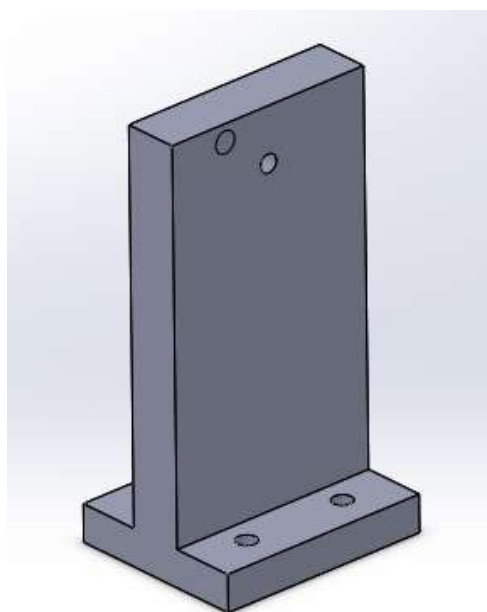
Figure 6.10: Support CAD

- Spring:

The spring is in charge of returning the mechanism to the initial position, as the piezo is not able to produce a traction force. The idea is to put a spring that can produce 500N, which is half the force that the piezo is able to produce. Considering that the compression of the spring is negligible, the force on the mechanism would always be the same on both movements (piezo and spring). To select the spring, we did a calculation:

$$25mm \cdot F_k = 1000N \cdot 1mm \quad (Eq.\ 6.1)$$

$$F_k = 40N$$

With some geometrical specifications, we found the right spring:

Table 6.2: *Spring characteristics (measures in mm)*

Material: cp: ALAMBRE DE ACERO EN 10270-1 SH-PH (DIN 17223/84-C)	
Total Length	65
Number of wires	1.00
Usefull spirals	21.00
External diameter	8.00
Internal diameter	6.00
Pitch	3.10
K (DaN/mm):	0.1475

The details of the exact designs of all the parts are specified in the planes, in the annex "**Drawings**".

- **Recovered parts from old set up**

- Fork

The fork structure has been optimized. The mass of the fork has been minimized so the moment of inertia of the rotating parts is reduced. Moreover, the structure should increase the flexural stiffness. Both aspects help to reduce the deflections in the fork tip, and the torsion of the shaft, which affects directly to the vibration of the wire. This vibration may introduce an error in a hypothetical particle beam measure. So, if this vibration is minimized, the measure would be more precise.
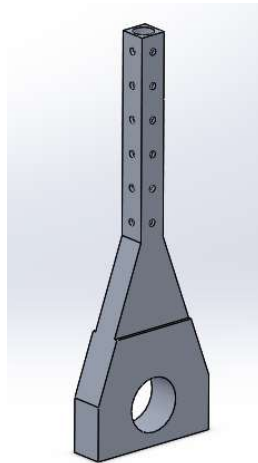
Figure 6.11: Shaft CAD

- Wire Fixing System

The wire fixing system consists of two pieces per fork. One piece is a small cylinder with two holes and it fits in the top of the fork. The other piece is a rectangle with a M1.6 threaded hole. The wire is placed between the two pieces and fixed with the 1.6 metric screw, (Figure 6.10)
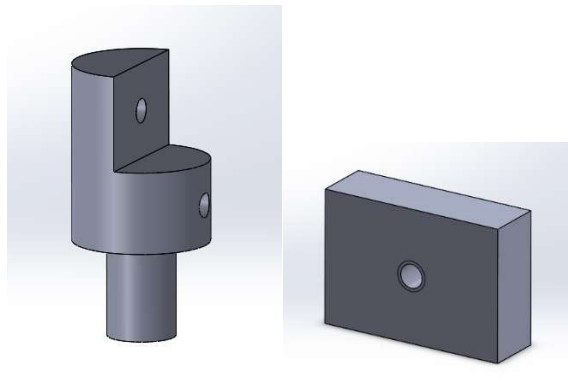
Figure 6.12: Wire fixing system CAD

- Carbon wire

A carbon wire is stretched between the forks, as the wire of the LHC scanner. The wire´s vibration measurement is based on its piezoresistive characteristics. The vibration of the fork and of the wire itself, changes the wire length and that produces a variation of the wire resistance. This variation is measured by a Wheatstone bridge, as has been done with the strain gauges, and it is directly proportional to the change of wire length. The conversion

coefficient and the rest of the wire characteristics are shown in the Table 6.3 **[2]**.

Table 6.3: *Wire characteristics and calibration coefficients*

Ø	Wire diameter	34	[μm]
ρ	Density	1800	[kg/m³]
L_0	Wire length	100	[mm]
k	Axial stiffness	340	[N/m]
F_{max}	Breaking force	0.5	[N]
R	Resistance	31	[Ohm/mm]
CL_W	Tension elongation coefficient	-0.35	[mm/V]
GF	Gauge factor	0.64	

- Semiconductor strain gauges

To measure de deflections of the fork arms, P type silicon semiconductor strain gauges are used (Figure 6.13). These gauges have more resolution than the standard resistive strain gauges. The specifications of the gauges used are shown in the Table 6.4 **[2]**. The position and the method to set them will be explained in the set-up assembly section.
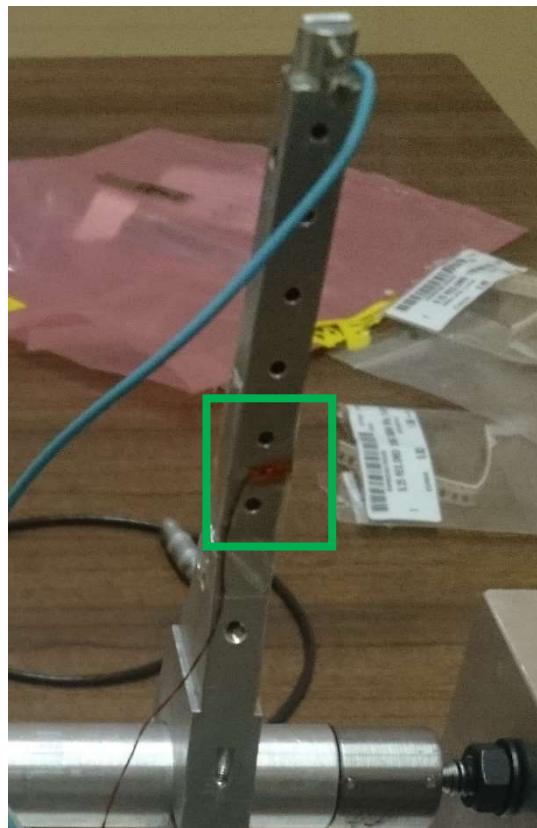
Figure 6.13: *Strain gauge detail*

Table 6.4*: Dimension and performances of semiconductor strain gauges*

Resistance [Ohm]	350
Dimension naked, length × width × thickness [mm]	$3.8 \times 0.2 \times 0.04$
Dimension baking, length × width × thickness [mm]	$5 \times 3.7 \times 0.05$
Gauge factor (GF)	$130 \pm 5\%$
TCR [1/°C]	$< 0.35\%$
TCGF [1/°C]	$< 0.28\%$
Maximum working current [mA]	10
Operating temperature range [°C]	$-50 \sim +80$
Fatigue life time [cycles]	$2 \cdot 10^6$
Strain limit [με]	6000

-   **Bought elements**

Hexagon Nuts

- ISO 4032 M6
- ISO 4032 M10

Hexagon socket head cap screw

- ISO 4762 M3x25
- ISO 4762 M4x25
- ISO 4762 M5x25

Hexagon socket head cap screw

- ISO 1207 M1.6x10

Other elements

- Ø6mm Steel ball
- Ø4mm Steel ball

6.2. Mechanism assembly

With all the necessary elements obtained, the mechanism is mounted. In order to ensure the correct functioning of the system, the assembly of the model will be explained step by step. We will use some pictures of the assembly as a help for the explanation.

To begin with, it is advisable to select a flat and levelled surface to place and fix the model.

ETSEIB

The prototype is assembled in two main subsets that will be joint together subsequently.

On the one hand there is the fixed set, formed by the feet, the base, the supports, the pointed screws, the springs screw with the spring and the screw for the piezoelectric actuator (the piezoelectric actuator is the only element that is mounted or dismounted when used).

On the other hand, there is the rotating set, formed by the shaft, the fork, the cam and the wire fixing system. The wire is not included in this set, and its insertion will be the last step of the process to prevent the wire from breaking due to its fragility.

First of all, we need to elevate the base to leave space between the base and the surface where it will be placed. This space will allow us to adjust the piezo and the spring later on. With this objective, the feet are fixed to the base using the ISO 4762 M5x25 screws, one for each foot.

Once the base set is ready, the next step will be to join the supports. Each support is fixed to the base with 4 ISO 4762 M5x25 screws.

Then, the fixed set is completed threading the pointed screws (Figure 6.14), the screw mechanized for the spring and the one for the piezo, each one with its corresponding locknut. The spring is placed in the mechanized part of the screw, in a way that allows compression and decompression and avoids buckling.

Figure 6.14: *Pointed screws detail view*

The focus now is on the rotating subset. The first thing that has to be done is to insert the hardened caps on the shaft. As explained in the designing section, it is recommendable to use a plastic mace to do this operation. Just place the cap on the shaft end and hit it with the mace until the gap between both parts disappears.

Next, the cam and both fork arms are introduced and fixed on the shaft, using ISO 4762 M3x25 screws. It is essential to ensure the position of those elements. The cam must be perfectly

centred, so it is aligned with the piezoelectric actuator and it does not undergo any strength moment. Also, the fork arms must be 100 millimetres apart and centred, thus the model is well balanced and undesirable inertial forces are avoided.

To finish with this subset, the wire fixing system has to be added (Figure 6.15). As the wire is in contact with this piece, it is used to connect the cables that will send the wire signal to the read-out system. Therefore, these pieces should not touch the fork arm. To guarantee this, we cover the piece with plastic and fix the piece with an insulating glue; any epoxy adhesive is acceptable.
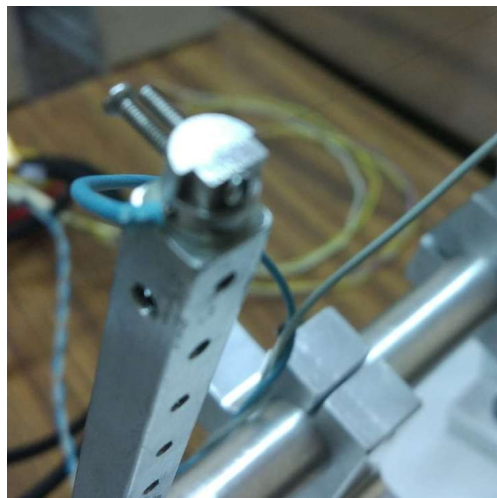
Figure 6.15: Wire fixing system and wire detail view

With both subsets completed, we can proceed to assembling them together. We insert the point of the screws, one after the other, then adjust both screws until the shaft is well positioned and able to rotate.

Then, adjust the height of the spring using its screw and introduce it into the cavity of the cam.

Now, the piezoelectric with balls at its contact points is introduced (Figure 6.16). That adds 3 degrees of freedom (rotation) to the movement of the piezo in such a way that it does not

undergo any moment.

Figure 6.16: Piezoelectric and spring assembly

Also, the strain gauges must be placed. The location selected is just over the change of section of the fork, since it is the most interesting point to study. The gauges are stick with an epoxy adhesive and covered with sticky tape to protect them.

Finally, the model is completed by carefully placing the carbon wire between the two pieces of the wire fixing system and screwing the ISO 1207 M1.6 screws.

To minimize the friction between moving parts in contact, a general lubricant can be used. In the present case, we have used a white lytic lubricant.

7. Experimental Set-Up

The experimental set-up consists not only of the mechanism, but also the measuring and signal generation chains. Part of the elements contained in those chains were available from the very beginning, while some others were not. In what follows, we describe and explain these elements and the construction of the chains.

7.1. Set-up elements

- ### Chain of generation and conditioning of the piezo signal

The piezoelectric is able to reproduce a movement pattern within a nanometer scale. So if we are able to send to it a signal that simulates the desired motion pattern, it will reproduce it with high precision. The signal must be generated and conditioned as follows (Figure 7.1):
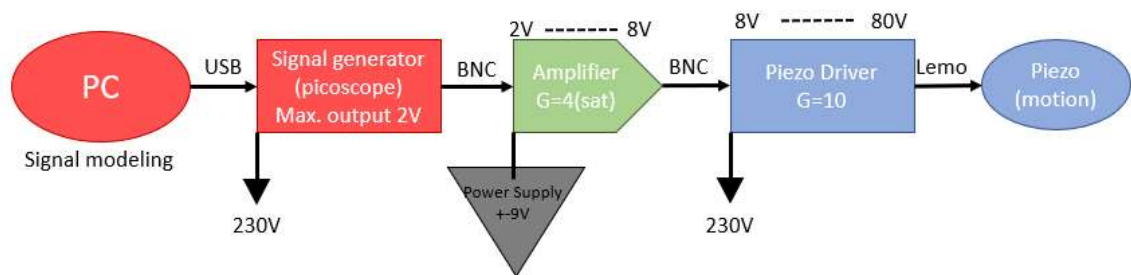
Figure 7.1*:Generation and conditioning chain´s blocks diagram*

- The signal is created with the PC in the Picoscope, which admits files with the .csv extension. We have written a simple program in Matlab to simulate the desired motion pattern.
- The signal must be amplified by an evaluation board. We use an EVAL-INAMP-82RZ model from Analog Devices. This board is can be used to evaluate different models of instrumentation amplifiers. For our project we are using the AD8429, that we have welded to the board. We have also welded both input and output BNC connectors and a 1.5k ohm resistor to obtain the gain desired, as specifies the Table 7.1 **[7]**.

Table 7.1: Gains achieved using 1% Resistors

1% Standard Table Value of R_G	Calculated Gain
6.04 kΩ	1.993
1.5 kΩ	5.000
665 Ω	10.02
316 Ω	19.99
121 Ω	50.59
60.4 Ω	100.3
30.1 Ω	200.3
12.1 Ω	496.9
6.04 Ω	994.4
3.01 Ω	1994

It must be supplied by two batteries of 9V each that we connect serially to obtain ±9V. With a 2V input, we can only get a gain of 4 because the board reaches a saturation point at 8V.

Figure 7.2: Amplification board

• The piezo driver reads and conditions the signal which is sent to the piezo and produces the desired movement.

- **Measurement chain**

The strain gauges resistance varies with the applied force. This happens when the fork deforms when moving. This resistance variation is measured and conditioned as follows (Figure 7.3):
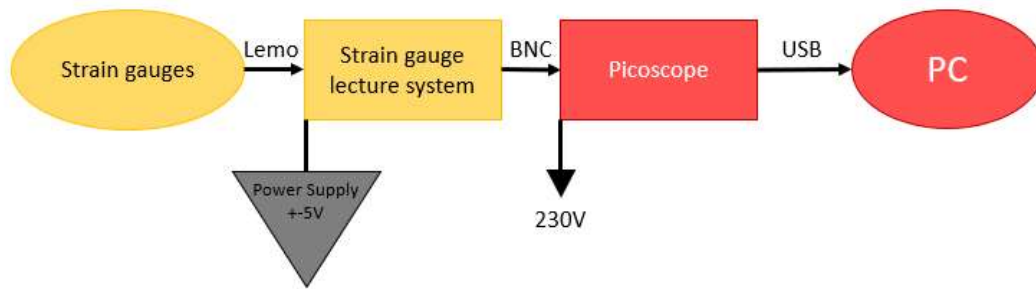
Figure 7.3: *Measurement chain´s blocks diagram*

- We use a 2 channel 5V power supply. By connecting those channels serially (Figure 7.4), we can obtain ±5V to supply the read-out system.
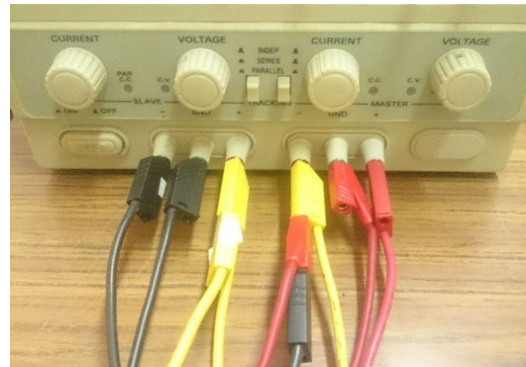
Figure 7.4: *Supply chain connection*

- The Wheatstone bridge must be balanced. With the potentiometer, we manage to put the output to zero, correcting any offset that could invalidate the measurement. The resistance variation causes bridge unbalance, and that translates into a potential difference.
- This voltage is measured and shown in the PC with the Picoscope.

The wire´s deformation measurement chain works exactly in the same way.

- Complete set up

Once we have all the necessary elements of our set up prepared, we can proceed to put them together and make the connections. The following figure, Figure 7.4, shows the complete set up, with all the connections before explained, ready to make measurements.
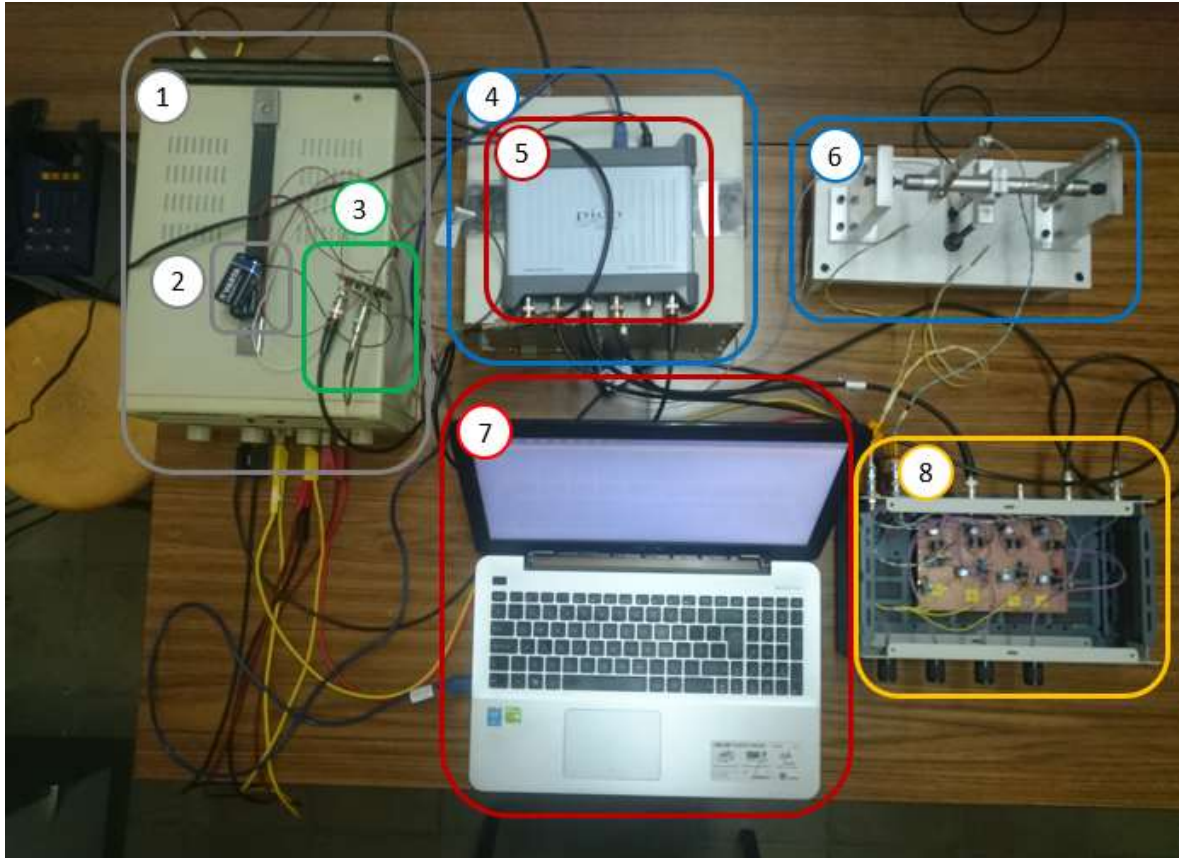
Figure 7.5:Complete set up

(1) Strain gauges lecture system´s power supply (2) Amplifier´s power supply (3) Amplifier (4) Piezo driver (5) Picoscope (6) Mechanism with the gauges and piezoelectric actuator (7) PC (8) Wire and strain gauges read out system

7.2. Set-up testing

Previous checks

The connections on the set up are not complex but the elements on it are delicate so it is advisable to check the voltage that provides the power supplies with a multimeter.

Once the first check is done, we can open the picoscope software on the PC and show the channels that we have connected on the picoscope. The signals must be centred on the 0. If not, check the state of the cables and eliminate the offset with the potentiometers.

Though the gauges have been checked before attaching them to the forks, they may undergo some damage during the connection process If they have not been damaged, we should be able to see a variation on the signal showed on the picoscope when moving the fork with a

finger (Figure 7.6).
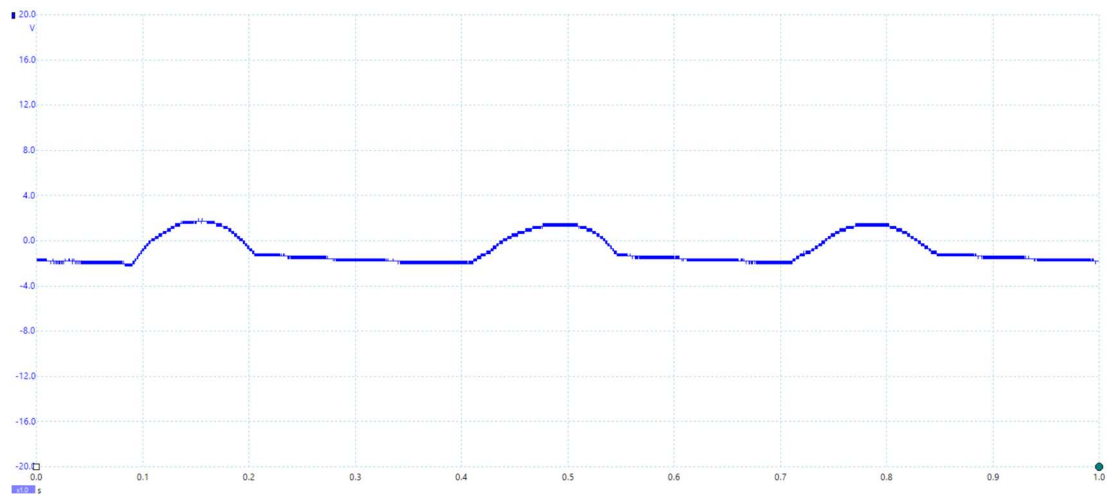
Figure 7.6*:Strain gauge operation check*

Each bump on the signal corresponds to an interaction between fork and finger. With this result we can conclude that the gauge is working.

First measurements

After making sure everything works as expected, we can proceed to introduce a signal to the piezoelectric actuator to see the system response in the PC. The signal created by the picoscope and sent to the actuator is a sinus with a 50 Hz frequency of excitation (Figure 7.7)
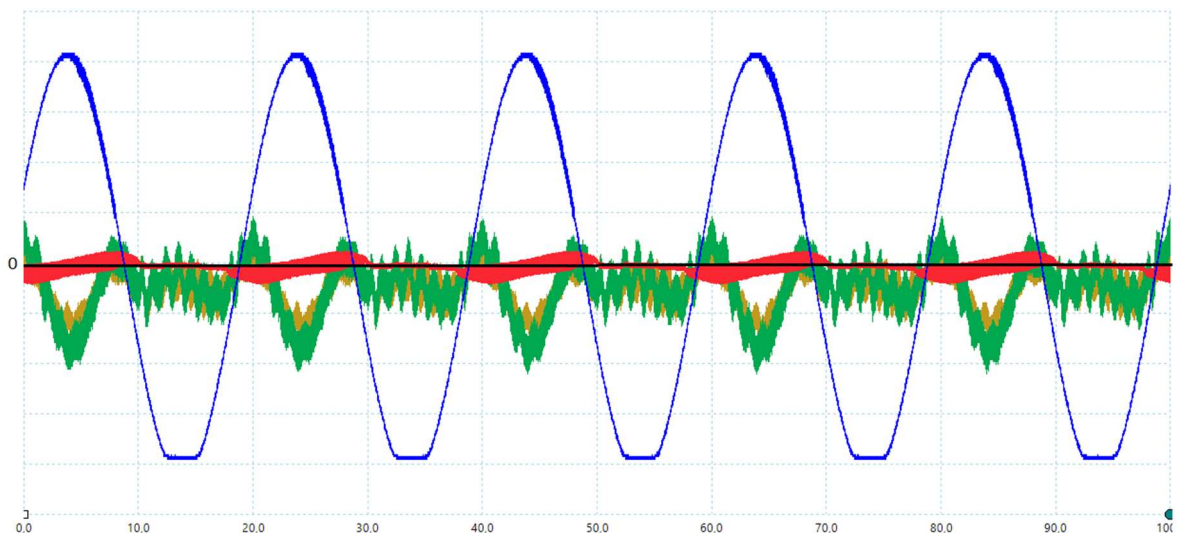
Figure 7.7*: Timescale:10ms/div. 50Hz sinus input measures. Generated signal (Blue), wire response (Red), left and right fork arms strain gauges response (Green and yellow)*

Figure 7.7 shows the first lecture of the gauges, the wire, and the signal sent to the piezo after

ETSEIB

the amplification board. From this picture we can highlight:

- The signal sent to the piezo shows a saturation point on ±8V.
- The behaviour of both strain gauges is similar.
- We see an important difference between the scales of each signals, but we cannot extract any conclusions because we have not yet applied the corresponding calibration factor.
- The three signals show a non-negligible noise so it would be advisable to apply a low pass filter.

When applying 1KHz low pass filter, the noise disappears, so we can appreciate better the response of the elements to understand their behavior (Figure 7.8).
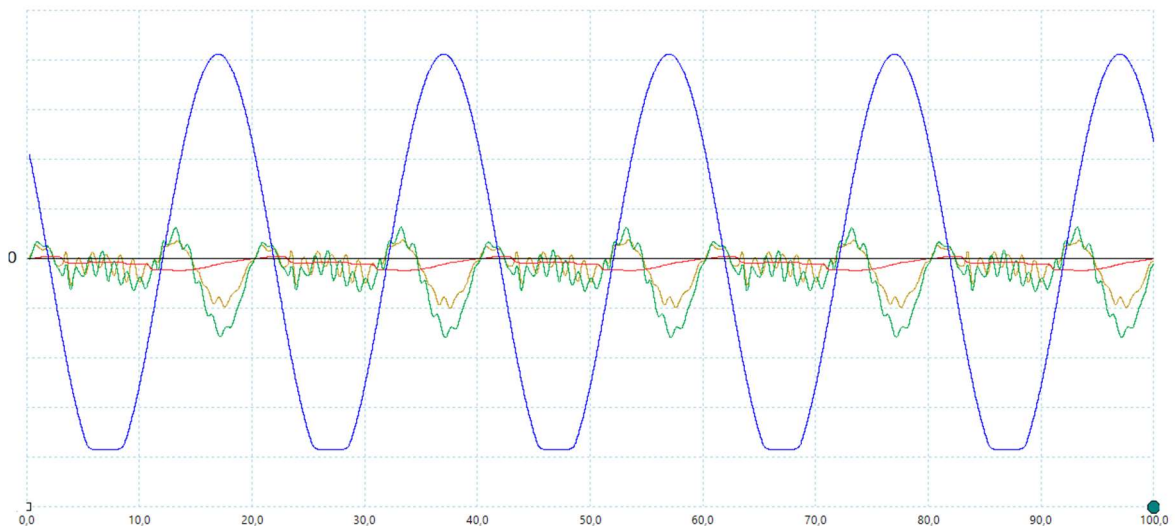
Figure 7.8*:Timescale:10ms/div. 50Hz sinus with 1KHz low pass filter. Generated signal (Blue), wire response (Red), left and right fork arms strain gauges response (Green and yellow)*

We can also proceed to a frequency analysis in order to make visible which are the most important frequencies on the system and whether those results meet the expectations (Figure 7.9).
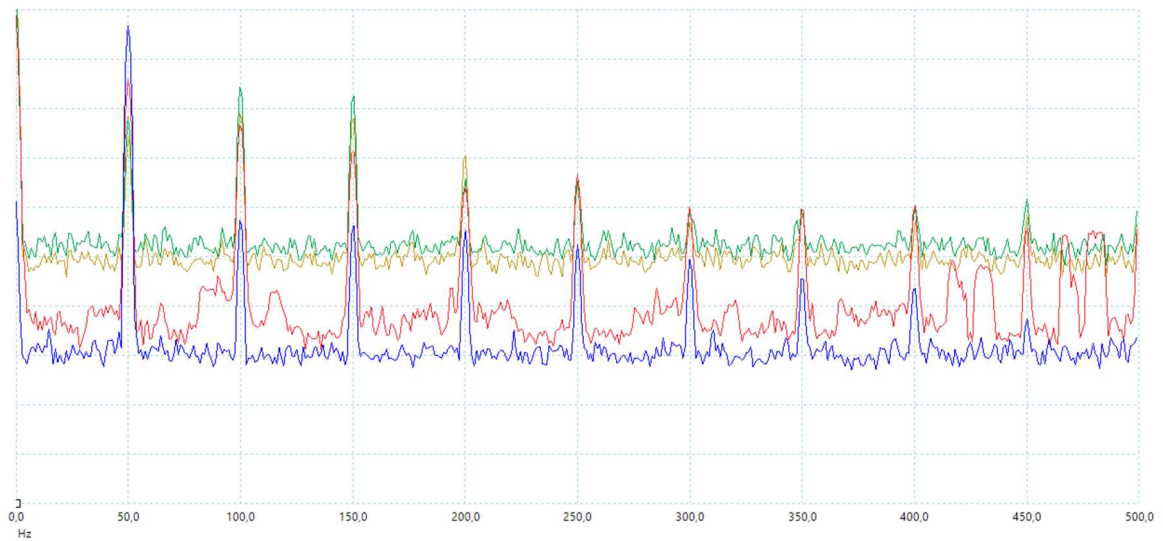
Figure 7.9: *Frequency scale: 50Hz/div. 50Hz sinus frequency analysis. FFT of the generated signal (Blue), wire response (Red), left and right fork arms strain gauges response (Green and yellow)*

We can clearly see the 50 Hz frecuency from the excitation and its different harmonics, so we can confirm that the system works as intented.

ETSEIB

8. Experimental Results

Once the setup is mounted and checked we can proceed to drive the system using the designed motion pattern, in order to analyze the results and understand the wire scanner behavior. It is important to note that this study is mostly qualitative and we are looking more for curve shapes rather than for specific values, as for now the system is not precise enough to carry out exact measurements and the low resolution does not allow to correct the signal offsets properly.

The Picoscope can generate any predefined cyclic signal at a chosen frequency. We joined the three phases of the motion pattern and their inverse, thus producing the complete OUT-IN / IN-OUT cycle described in chapter 3.1. We also added a rest phase before and after each cycle in order to visualize the free oscillation of the system. Figure 8.1 shows the wire response as a variation of its resistance (red) to a 50 Hz cyclic excitation (blue):
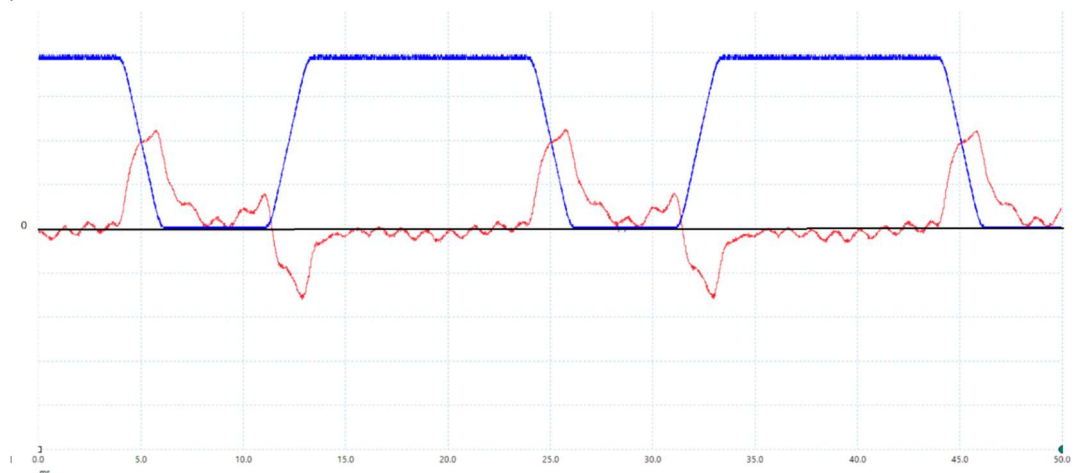
Figure 8.1:Timescale: 5ms/div. 50 Hz excitation (Blue), wire resistance variation (Red).

The results are not what we expected. As the tension-elongation factor of the wire is negative (Table 6.3), the wire length variation is shown as a negative voltage for stretches and as a positive one for contractions. According to the simulation the wire displacement should reproduce Figure 5.13 during the OUT-IN and IN-OUT motion and a free oscillation on the steady phases, but only the latter is accomplished in the previous result.

The main problem is the presence of positive values, especially on the peak on the IN-OUT motion, as it should be negative and equal to the response on the OUT-IN. If the whole system were rigid (except the wire), the variation of the wire length would be always positive and it should be seen in the oscilloscope as a negative tension. This problem reveals that there must be some reason besides the fork motion that modifies the wire length, allowing its shortening (which would justify the positive tensions observed in Fig. 8.1).

The first hypothesis we have is to attribute this wire length modification to a deformation of the fork arms, but we quickly discard it for various reasons. First of all, a fork deformation in the wire longitudinal direction is not possible, as the motion is rotational and it can mainly cause deflections perpendicular to the wire. This perpendicular deformation could explain a wire length increase (in a case of the fork arms oscillating in counter phase), but never a contraction as the minimum separation corresponds to a complete alignment between both arms and the wire.

The main scenario we have on this matter is that it is caused by a deformation of the shaft that holds the fork. The shaft direction is the axis of the rotational movement and should be its only degree of freedom if it did not undergo any deformation, as every other possible movement is restricted by the screws in its extremes.

As the Piezoelectric actuator applies its force on the middle point between the extremes of the shaft and really close to the axis, it is plausible that the shaft suffers a deformation (similar to what happens to constructive beams) provoking a separation of the fork tips (Figure 8.2). Then, as the system cycles repetitively it would generate an oscillation to the shaft that would transmit into cyclic variations of the wire length.
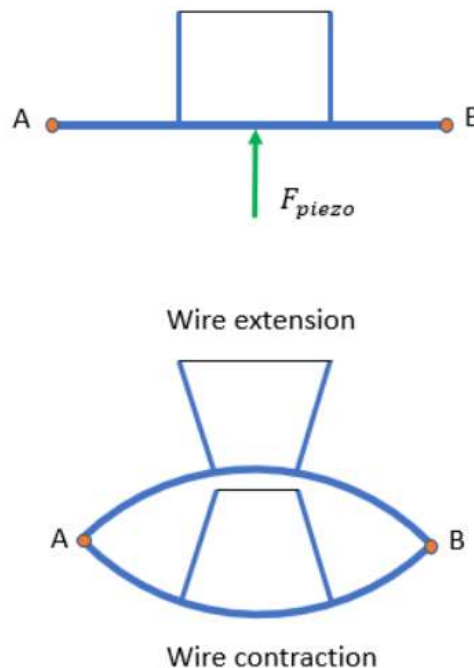
Figure 8.2: *Deformation of the shaft in response to the actuator motion*

To verify this hypothesis, we installed a strain gauge on the middle point of the shaft, aligned

with the fork, as it is where the highest deformation should happen. The first test we carried out was introducing a square signal to the system and comparing the behavior of the wire and the shaft strain gauge (Figure 8.3).
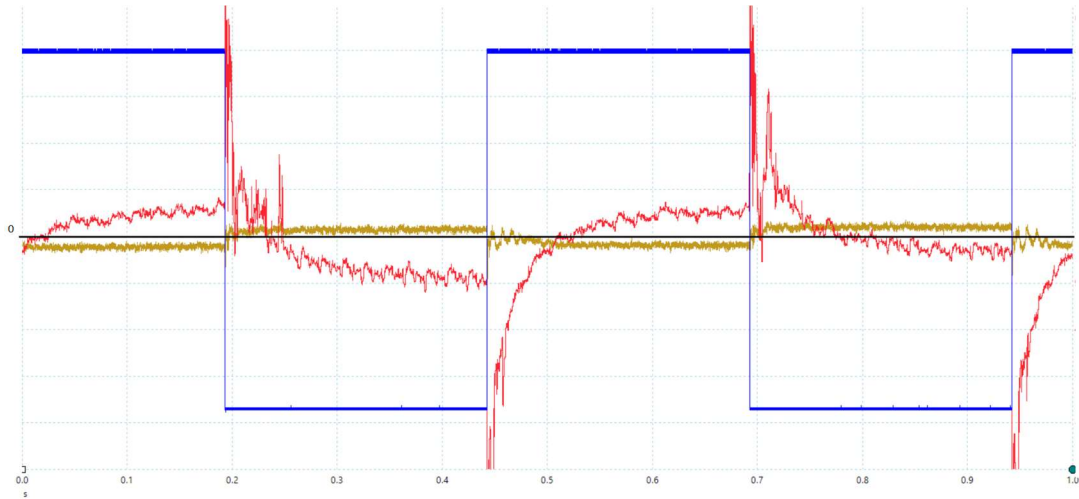
Figure 8.3*: Timescale 0.1s/div. Square signal (Blue), wire response (Red), shaft strain gauge (Yellow).*

Observing the results, we increase the suspect that the wire length variation is significantly influenced by the deformation of the shaft. The variation of the voltage of the shaft strain gauge is consistent with the hypothesis in Figure 8.2, as it is negative in the rise flank (when the shaft bends upwards, the strain gauge stretches) and positive in the lowering flank (when the shaft bends downwards, the strain gauge compresses). The variation of voltage of the wire acts in the same way, which should not happen without the shaft deformation.

To further confirm the hypothesis, we proceed to execute a similar test but now with the designed motion pattern (in blue in Figure 8.4) with an excitation frequency of 90 Hz. The result is filtered with a 1kHz low-pass filter so that the high frequency vibrations of the wire are hidden and we can better compare its behavior with the shaft deformation, which oscillates much slowly.
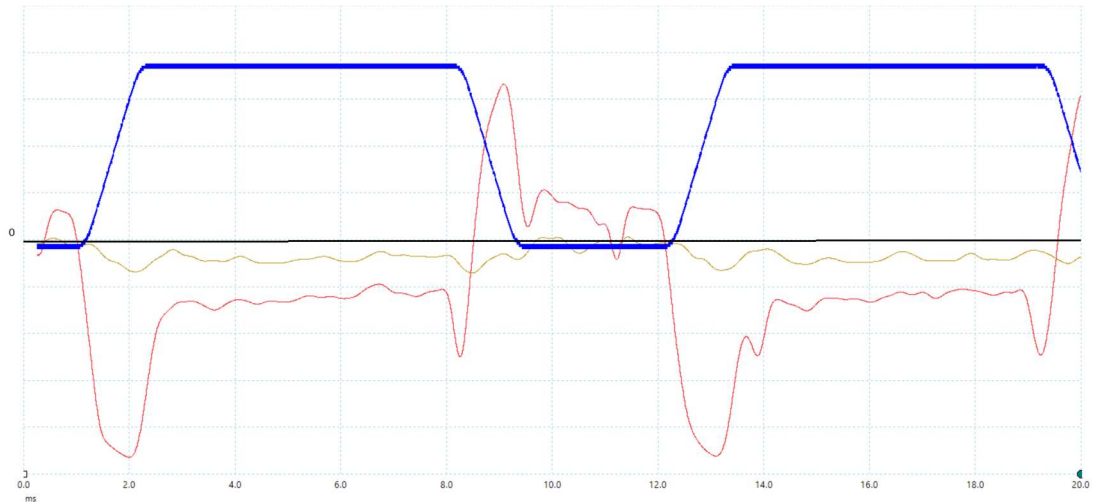
Figure 8.4*: Timescale: 2ms/div. 1KHz low pass filter. Motion pattern signal (Blue), wire response (Red), shaft strain gauge (Yellow).*

We can now confirm the aforementioned hypothesis, as comparing the wire and shaft gauge signals it is obvious that their behavior is correlated. During the steady phases the wire performance is completely proportional to the shaft deformation and there are only differences during the fork motion, which can be logically explained.

In the OUT-IN motion there is a single negative voltage peak, as the shaft deformation and the wire displacement both contribute to a length increase. However, in the IN-OUT motion there is first a small negative peak which is then followed by a higher positive peak. This shows that first the wire displacement dominates but once the shaft deforms enough it prevails, thus decreasing the wire length and appearing as a positive voltage.If we remove the low-pass filter, we recover the high frequency vibration of the wire (Figure 8.5):
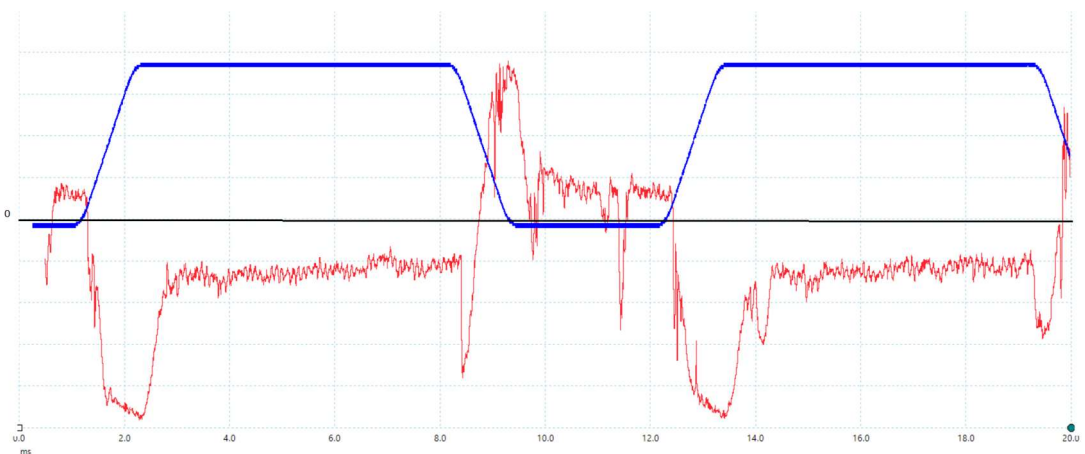
Figure 8.5*: Timescale: 2ms/div. Signal without low pass filter. Pattern signal (Blue), wire response (Red)*

ETSEIB

Finally, we performed an FFT of the wire elongation and shaft deformation signals (Figure 8.6 and Figure 8.7) to analyze their frequency spectrum and identify the most relevant components of their oscillation.
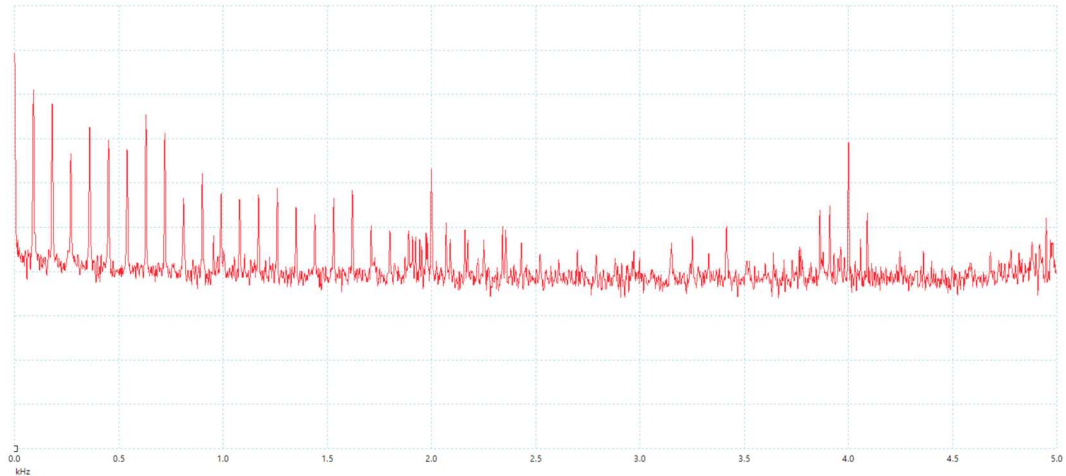
Figure 8.6*:Frequency scale: 0.5KHz/div. Frequency analysis. FFT of the wire signal*
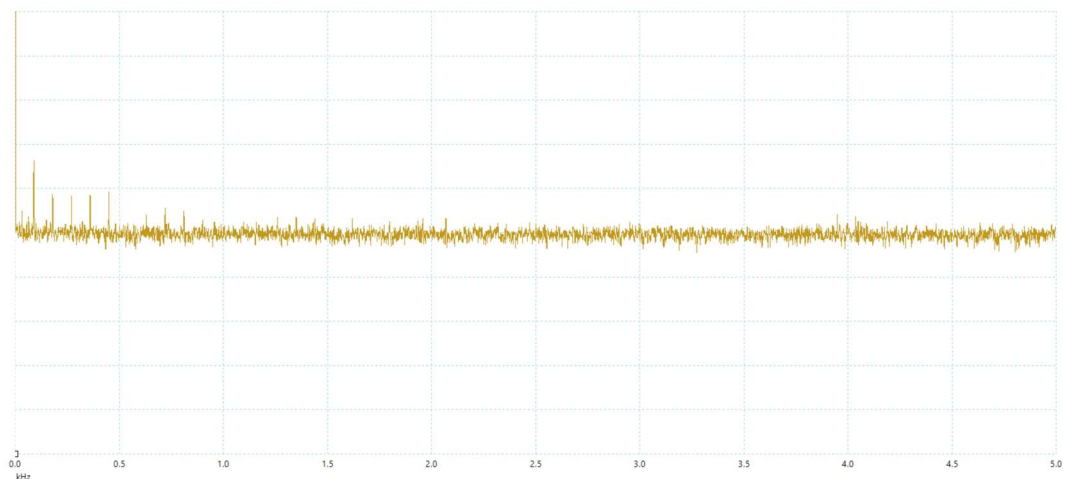
Figure 8.7*:Frequency scale: 0.5KHz/div. Frequency analysis. FFT of the shaft strain gauge signal*

We can see in both signals the presence of the 90 Hz frequency and its harmonics. This component was expected as it is the excitation frequency of the imposed motion cycle. Additionally, on the wire signal we can observe an important peak at 2 kHz and its first harmonic at 4 kHz. We suspect that this corresponds to the first vibration mode of the wire (given by $f = \frac{1}{4L_0}\sqrt{\frac{F_0}{\mu_0}}$), which should be around 1,25 kHz with the parameter values considered in the simulation. However, as in the real system we are not able to exactly measure them (especially the initial tension L_0), we think that it could vary up to the 2 kHz that can be appreciated in the frequency spectrum.

Project schedule and costs

Budget

I. Materials Costs

Description	Number	Unit cost €/u	Total Cost €
Aluminium 7075 15x140x300 plate	1.8	5.90	10.62
Aluminium 7075 60x70x120 plate	2	10.00	20.00
Aluminium 7075 15x50x70 plate	1	6.00	6.00
Aluminium 7075 Ø25x200 bar	1	6.00	6.00
Compression spring Ø8x65	1	16.30	16.3
DIN 933 12.9 M6x35 screw	3	0.31	0.93
DIN 933 8.8 M10x80 screw	1	1.00	1.00
DIN 912 12.9 M4x25 screw	8	0.26	2.08
DIN 912 12.9 M5x25 screw	4	0.29	1.16
DIN 934 M6 nut	3	0.08	0.24
DIN 934 M10 nut	1	0.37	0.37
DIN 125 M6 washer	3	0.05	0.15
DIN 125 M10 washer	1	0.15	0.15
Manufacture costs	1	480	480
Electronic elements used cost (approx.)	1	10000	10,000
Others (lubricant, glue…)	1	15	15
TOTAL			10,560 €

Design, implementation and testing of a wire scanner prototype   Pàg. 69

II.   Engineering Costs

Description	Hours	Unit cost €/h	Total Cost €
Engineer 1	300	50	15,000
Engineer 2	300	50	15,000
TOTAL			30,000 €

ETSEIB

Gantt chart

Gantt chart (2019)

- 13 Feb — Project Inscription
- 11 Feb-13 Feb — First talks
- 13 Feb - 15 March — Draft Scope
- 20 Feb – 1 March — Previous documentation study
- 15 March– 26 April — Mechanism Design
- 5 April - 4 June — Wire model and movement pattern design
- 1 May — Planes sent to manufacturers
- 22 May - 8 July — Piezoelectric actuator and strain gauge+wire's electronics commissioning
- 10 June — Pieces arrival
- 24 Jun — Evaluation board arrival
- 10 June – 3July — Mechanism assembly
- 10 June – 3July — Complete Set-up
- 18 July – 1 Aug — Previous checks and first measures
- 1 Sept – 20 Sept — Final measures and conclusions
- 20 Sept — Project Sign-Off

Conclusions

The main goal of this project was to design and implement a prototype to reproduce the LHC original wire scanner, being able to carry out measurements of the wire motion to help understanding and minimizing its vibration. We can assert that the objectives have been accomplished, as the final results are qualitatively satisfactory though the system will need future adjustments in order to allow precise quantitative measurements.

An initial viability study has been carried out to define a possible mechanical solution for the prototype. The main drawback has been the usage of a Piezoelectric linear actuator, which has a really short stroke that strongly limited the constructive possibilities. Through this study it has been decided to implement a rotary set up using a cam to transform the linear movement of the actuator to a rotation.

A mechanism for the prototype has been engineered, manufactured and assembled to fulfill the system requirements. The design of the mechanism has been done taking into account both economic and time restrictions, so it might be not as precise as would be desirable. Even so, it has been done a good design and the mechanism has been functional for this project. The majority of the parts have been designed and modeled in 3D CAD software, and then drawn in technical plans in order to be mechanized in aluminum using CNC machining. The system works as intended, although its movement is pretty restricted by the Piezoelectric actuator.

The dynamics of the wire in the wire scanner have been modelled, understood and simulated to assess its response to different excitation patterns. A simple motion pattern has been proposed, with the intention to smooth the fork behavior and minimize the wire vibrations. A simulation has been carried out using Matlab programming, combining the wire motion equations with the motion pattern to predict the performance of the system and to compare it with the measurements.

An experimental set-up has been installed in order to drive and measure the system. A picoscope with the support of a computer has been used both to generate the motion pattern signal and to read the system response. A conditioning chain with a driver and an amplifier has been connected to adapt de signal for the actuator. A measurement chain has been installed to read the electric signal from the wire and from different strain gauges mounted on the mechanism to measure its deformation.

Finally, some experimental tests have been carried out to validate the performance of the prototype. The tests outcomes have been compared with the previous simulation to evaluate their reliability and identify possible sources of error.

ETSEIB

The results of the tests show that the system performance has some important differences with what we expected from the mathematical model and simulation. The most important disparity is the reading of positive voltages from the wire signal, which indicates the presence of length contractions during the motion although in theory the wire should only undergo positive length variations.

The main hypothesis for this problem is the existence of a deformation of the shaft that would cause the fork to open and close cyclically, thus altering the length of the wire. This scenario has been qualitatively verified through measurements through a strain gauge mounted on the shaft. The gauge readings and their comparison to the wire resistance measurements confirm that the wire performance is strongly influenced by the shaft deformation.

For future works this problem needs to be addressed to allow a proper operation of the system. Different materials should be tested for the shaft to increase its stiffness and thus minimize its deformation. Furthermore, the wire dynamic model should be improved, adding another degree of freedom to convert it into 3DOF system by taking into account the possibility of the shaft deformation.

In conclusion, we believe that a pretty good work has been done and, although it needs some adjustments, the constructed prototype works properly and will be able to help enlarging the knowledge about the wire scanner. The next step in this subject should be the optimization of the motion pattern in order to minimize the wire vibrations. The prototype should be used to carry out the needed tests, but we first recommend to solve the shaft deformation problem and to change the piezoelectric actuator for a larger stroke one.

ETSEIB

Acknowledgements

To the directors of the project, Ana Barjau and Juan Herranz, for all the help, guidance and experience given to us during the process of this project. The amount of time they have inverted in this task is unpayable, and it is safe to say that without their assistance we would not have been able to complete this challenge.

To the CERN Beams and Instrumentation department for providing the necessary material for the implementation of the wire scanner prototype. We would like to especially acknowledge Jonathan Emery and Federico Roncarolo for sharing their knowledge and giving remote help whenever needed.

To the ETSEIB professors Daniel Clos, Joaquim Veciana, Juan Manuel Moreno and Carles Domenech for unselfishly assist us in the different disciplines present in the project.

To the ETSEIB manufacturing workshop, particularly to Rafael Bermudez and Irene Buj for counselling us during the process of fabrication.

Finally, to our friends and relatives for their support and patience throughout this journey.

Bibliography

Bibliographic references

[1] Juan Herranz, Ana Barjau, Bern Dehning, Minimisation of the wire position uncertainties of the new CERN vacuum wire scanner, PhD Thesis, January 2016.

[2] Juan Herranz, Ana Barjau, Bernd Dehning, *Vibration measurements of a wire scanner – Experimental setup and models*. Elsevier, March 2016.

[3] Ana Barjau, Juan Herranz, Bern Dehning, *Dynamical Models of a Wire Scanner,* Journal of Vibration and Acoustics, October 2016, Vol.138.

[4] Alejandro Copetudo, Ana Barjau, *Optimizació del patró de rotació d´un escáner del fil*, July 2016.

[5] UNE-EN ISO 286-1:2011

[6] Salvador Cardona Foix, Daniel Clos Costa, *Teoría de máquinas,* Ediciones UPC, February 2001

[7] Analog Devices, *AD8429 datasheet*, One technology way, 2017.

ETSEIB